Defence Research and Development Canada
Recherche et développement pour la défense Canada

DEFENCE R&D DÉFENSE

Adaptive Processing of RADARSAT-1 Fine Mode Data

Ship Parameter Estimation

Paris W. Vachon and Marina Dragošević

Defence R&D Canada – Ottawa
TECHNICAL MEMORANDUM
DRDC Ottawa TM 2007-053
March 2007

Canada

Adaptive Processing of RADARSAT-1 Fine Mode Data

Ship Parameter Estimation

Paris W. Vachon
DRDC Ottawa

Marina Dragošević
Terrabytes Consulting

Defence R&D Canada – Ottawa

Technical Memorandum
DRDC Ottawa TM 2007-053
March 2007

Principal Author

Original signed by Paris W. Vachon

Paris W. Vachon

Defence Scientist

Approved by

Original signed by Gary W. Geling

Gary W. Geling

Head, Radar Applications and Space Technologies Section

Approved for release by

Original signed by Cam Boulet

Cam Boulet

Chair, Document Review Panel

This work was supported in part by a Service Level Agreement between the Polar Epsilon Project Management Office and Defence R&D Canada - Ottawa.

© Her Majesty the Queen as represented by the Minister of National Defence, 2007

© Sa Majesté la Reine, représentée par le ministre de la Défense nationale, 2007

Abstract

The Chip-based Adaptive synthetic aperture radar (SAR) Processor (CHASP) was developed to facilitate the precision processing of airborne SAR data of moving ship targets. CHASP has been extended to support the processing of RADARSAT-1 (R-1) Range Compressed (RC) data and applied to a set of 121 known ships in R-1 Fine mode data.

It is shown that, for R-1 Fine mode data, CHASP-like algorithms can provide more ship information than can be deduced from image analysis alone. Based upon comparison of the ship residual frequency with the Doppler centroid of the background clutter, the ship radial speed can be estimated to within ±2 m/s. Azimuth travelling ships are the most difficult cases for length and speed estimation, but azimuth travelling ships can be readily recognised through a high modulation index of the power envelope in azimuth. The ship radar cross section (RCS) is well estimated for both range and azimuth travelling ships. Unfortunately, processing experiments could neither prove nor refute the expected SAR resolution dependence of the measured ship RCS.

Single look complex (SLC) data could also be used as a starting point for CHASP-like analysis. However, this would introduce additional complexity since the internal details of the SAR processor must be completely known. In general, it is recommend that adaptive ship data analysis start from RC data.

The most important outcome of this work is that, for R-1 Fine mode data, frequency tracking of the ship signature can provide an accurate estimate of the ship radial speed under generalized conditions. Normally, ship radial speed estimation relies upon the azimuth shift of the ship target relative to the ship wake location. Unfortunately, ship wakes are rather rarely visible in R-1 data.

Résumé

Le processeur de radar à synthèse d'ouverture (SAR) adaptatif à puce (CHASP) a été mis au point dans le but de faciliter le traitement de précision des données de radar SAR aéroporté sur des navires cibles en mouvement. Le CHASP a été étendu de manière à prendre en charge le traitement des données à compression de portée de RADARSAT-1 (R-1) et appliqué à une série de données sur 121 navires connus en mode Fin de R-1.

On montre que, dans le cas des données en mode Fin de R-1, les algorithmes de type CHASP peuvent fournir plus d'information sur les navires que ce qu'on peut déduire uniquement de l'analyse des images. D'après une comparaison de la fréquence résiduelle d'un navire avec le centroïde Doppler du clutter de fond, la vitesse radiale du navire peut être estimée à ± 2 m/s. Les navires en déplacement en azimut représentent les cas les plus difficiles d'estimation de la longueur et de la vitesse, mais ils peuvent facilement être reconnus au moyen d'un indice de modulation élevé de l'enveloppe de puissance en azimut. La surface équivalente radar est bien estimée pour les navires en déplacement en azimut et en portée. Malheureusement, les expériences de traitement n'ont pas permis de prouver ni de réfuter la dépendance attendue à l'égard de la résolution du radar SAR de la surface équivalente radar de navire mesurée.

Des images complexes singulières ont également pu être utilisées comme point de départ d'une analyse de type CHASP, ce qui a cependant pour effet d'introduire une complexité additionnelle, du fait que les détails internes du processeur de radar SAR doivent être connus au complet. En règle générale, on recommande de faire débuter l'analyse de données de radar adaptatif par les données à compression de portée.

Le résultat le plus important du travail est le fait que, dans le cas des données en mode Fin de R-1, la poursuite en fréquence de la signature d'un navire peut fournir une estimation précise de la vitesse radiale du navire dans des conditions générales. Normalement, l'estimation de la vitesse radiale du navire dépend du déplacement en azimut du navire cible par rapport à l'emplacement de son sillage. Malheureusement, il est plutôt rare que les sillages de navires soient visibles dans les données de R-1.

Executive summary

Adaptive Processing of RADARSAT-1 Fine Mode Data: Ship Parameter Estimation

Vachon, P.W., Dragošević, M.; DRDC Ottawa TM 2007-053; Defence R&D Canada – Ottawa; March 2007.

Introduction

The Chip-based Adaptive synthetic aperture radar (SAR) Processor (CHASP) was developed to facilitate the precision processing of airborne SAR data of moving ship targets. CHASP contains many analysis algorithms and has proven to be useful in reducing the adverse effects of vessel motion and producing better focused images of ships for downstream analysis.

Although the acquisition geometry and velocity sensitivity are very different for spaceborne versus airborne SARs, this document summarizes efforts to extend CHASP to the processing and analysis of RADARSAT-1 (R-1) data. Specifically, CHASP was extended to accept Range Compressed (RC) data from a commercial SAR processor. CHASP was then used to analyze a data set comprised of 121 known ships in R-1 Fine mode imagery. The ship identification and velocity validation data were available via Automatic Identification System (AIS) data obtained from AISLive.

Results

The following results are based upon the analysis of a statistically significant number of ship targets in R-1 Fine mode RC SAR data:

- CHASP can provide useful ship information for R-1 SAR through use of a fast, chip-based analysis;
- Based upon comparison of ship residual frequency with the Doppler centroid of the background clutter, the ship radial speed can be estimated to within ±2 m/s;
- The Map-drift and similar algorithms are probably not reliable enough for R-1 processing;
- Estimation of vessel orientation from the ship signature is possible, at least for vessels over 50 m in length in R-1 Fine mode data;
- Aspect angle estimation may be ambiguous, especially for slow moving or azimuth travelling ships;
- Azimuth travelling ships are readily recognised through azimuth elongation of the ship signature in the image domain, a high modulation index of the power envelope in azimuth, and a low confidence measure for the aspect angle estimate;
- Azimuth travelling ships are the most difficult cases for length and speed estimation;

- Ship radar cross section (RCS) is well estimated for both range and azimuth travelling vessels;
- When ship RCS is estimated from multi-look images, the look normalization strategy may influence the results; and
- The processing experiments carried out could neither prove nor refute the expected SAR resolution dependence of the measured ship RCS.

Significance

CHASP was initially developed for processing of airborne SAR data. CHASP was subsequently revised to provide geo-referencing and calibrated data for the R-1 case. Not all CHASP algorithms apply to spaceborne SAR data, but the analysis shows that significantly more ship information is available by using adaptive processing algorithms than can be deduced from image analysis alone.

Most of the analysis was carried out using range-compressed (RC) data, rather than single look complex (SLC) data, a product type that is routinely available from commercial SAR processors. While most of the algorithms considered could work with SLC data, additional complexity is introduced since the internal details of the SAR processor must be completely known. It is recommended that adaptive ship data analysis start from RC data.

The most important outcome of this work is that, for R-1 data, frequency tracking of the ship signature relative to the background clutter can provide an accurate estimate of the ship radial speed under broad conditions. Normally, radial speed estimation relies upon the azimuth shift of the ship target relative to the ship wake location. The problem with the ship wake approach is that wakes are rather rarely visible in R-1 data. The frequency tracking method does experience problems when the background clutter level is very low.

Future plans

While the analysis in this document has focussed on R-1 Fine mode data, it should be noted that the CHASP algorithms should apply equally well to lower resolution modes, as will be adopted for operational maritime surveillance using RADARSAT-2. It is recommended that CHASP-like algorithms be considered for operational use in this context, with RC data as the starting point for CHASP-like processing. In support of this objective, additional tests with lower resolution data are recommended.

Sommaire

Adaptive Processing of RADARSAT-1 Fine Mode Data: Ship Parameter Estimation

Vachon, P.W., Dragošević, M.; DRDC Ottawa TM 2007-053; R & D pour la défense Canada – Ottawa; mars 2007.

Introduction

Le processeur de radar à synthèse d'ouverture (SAR) adaptatif à puce (CHASP) a été mis au point dans le but de faciliter le traitement de précision des données de radar SAR aéroporté de navires cibles en mouvement. Il contient de nombreux algorithmes d'analyse et s'est avéré utile en vue de la réduction des effets néfastes des mouvements des navires et de la production d'images plus claires de navires en vue de leur analyse en aval.

Bien que la géométrie d'acquisition et la sensibilité de la vitesse soient très différentes dans le cas des radars SAR spatiaux par rapport aux radars SAR aéroportés, le présent document résume les efforts déployés pour étendre le CHASP au traitement et à l'analyse de données de RADARSAT-1 (R-1). Plus précisément, le CHASP a été étendu de manière à accepter les données à compression de portée d'un processeur SAR commercial. Le CHASP a alors servi à l'analyse d'une série de données composée d'images de 121 navires connus obtenues en mode Fin de R-1. Les données d'identification des navires et de validation de leur vitesse étaient disponibles au moyen de données d'un système d'identification automatique (SIA) obtenues d'AISLive.

Résultats

Les résultats qui suivent ont été obtenus à partir de l'analyse d'un nombre statistiquement important de navires cibles dans des données de R-1 en mode Fin de radar SAR à compression de portée:

- Le CHASP peut fournir des données utiles sur les navires pour le radar SAR R-1 grâce à l'utilisation d'une analyse rapide à puce;
- D'après une comparaison de la fréquence résiduelle d'un navire avec le centroïde Doppler du clutter de fond, la vitesse radiale du navire peut être estimée à ± 2 m/s;
- Les algorithmes de dérive cartographiques et des algorithmes semblables ne sont probablement pas assez sûrs pour le traitement de données de R-1;
- L'estimation de l'orientation d'un navire à partir de sa signature est possible, du moins dans le cas des navires de plus de 50 m dans des données en mode Fin de R-1;
- L'estimation de l'angle d'aspect peut être ambiguë, en particulier dans le cas des navires en déplacement en azimut ou en mouvement lent;
- Les navires en déplacement en azimut sont facilement reconnaissables par l'allongement en azimut de leur signature dans la représentation en image, étant donné un indice élevé de

modulation de l'enveloppe de puissance en azimut et une mesure de confiance peu élevée à l'égard de l'estimation de l'angle d'aspect;

- Les navires en déplacement en azimut représentent les cas les plus difficiles d'estimation de la longueur et de la vitesse;
- La surface équivalente radar est bien estimée dans le cas des navires en déplacement en portée et en azimut;
- Lorsque la surface équivalente radar de navire est estimée à partir d'images plurielles, la stratégie de normalisation de l'apparence risque d'influer sur les résultats;
- Les expériences de traitement qui ont été menées n'ont pas permis de prouver ni de réfuter la dépendance attendue à l'égard de la résolution du radar SAR de la surface équivalente radar de navire mesurée.

Importance

Le CHASP a été initialement mis au point en vue du traitement de données de radar SAR aéroporté. Il a par la suite été révisé de manière à fournir des données géoréférencées et étalonnées pour le cas de R-1. Ce ne sont pas tous ses algorithmes qui s'appliquent aux données de radar SAR aéroporté, mais l'analyse montre qu'il y a beaucoup plus de données disponibles sur les navires lorsqu'on se sert d'algorithmes de traitement adaptatif que ce qu'on peut déduire uniquement de l'analyse d'images.

L'analyse a été menée en grande partie au moyen de données à compression de portée, plutôt qu'à l'aide de données complexes singulières, qu'offrent couramment les processeurs SAR disponibles sur le marché. Même s'il était possible d'utiliser la plupart des algorithmes considérés avec les données complexes singulières, une complexité additionnelle est introduite, du fait que les détails internes du processeur SAR doivent être connus au complet. On recommande de faire débuter l'analyse des données de navire par les données à compression de portée.

Le résultat le plus important du travail est le fait que, dans le cas des données en mode Fin de R-1, la poursuite en fréquence de la signature d'un navire peut fournir une estimation précise de la vitesse radiale du navire dans des conditions générales. Normalement, l'estimation de la vitesse radiale du navire dépend du déplacement en azimut du navire cible par rapport à l'emplacement de son sillage. Le problème que pose l'approche axée sur les sillages, c'est qu'il est plutôt rare que les sillages de navires soient visibles dans les données de R-1. La méthode de poursuite à l'aide de la fréquence pose des difficultés lorsque le clutter de fond est très faible.

Perspectives

Bien que l'analyse ait porté, dans le présent document, sur les données en mode Fin de R-1, il est à noter que les algorithmes du CHASP devraient s'appliquer aussi bien aux modes à résolution moindre, et qu'ils seront adoptés pour la surveillance maritime opérationnelle à l'aide de RADARSAT-2. On recommande d'envisager des algorithmes du type CHASP en vue d'une utilisation opérationnelle dans ce contexte, les données à compression de portée constituant le point de départ du traitement de type CHASP. À l'appui de cet objectif, on recommande de mener d'autres essais à une résolution moindre.

Table of contents

Abstract i
Résumé ii
Executive summary iii
Sommaire v
Table of contents vii
List of figures viii
List of tables xii
Acknowledgements xiii
1. Introduction 1
2. Data processing 3
    2.1 Added CHASP functionality 3
    2.2 Processing procedure 4
3. Data 6
    3.1 RADARSAT-1 6
    3.2 AIS 7
4. Ship analysis results 11
    4.1 Georeferencing 11
    4.2 Radial speed 11
    4.3 Aspect angle 13
    4.4 Along-track speed 18
    4.5 Length 22
    4.6 Focus 25
    4.7 Radar cross section 28
5. Conclusions 39
Annex A σ° Maps 41
Annex B CDC Maps 45
Annex C CDC Transects 49
Annex D Examples of Processed Ships 53
Annex E Georeferencing Comparisons 57
Annex F Radial Speed Error Histograms 61
Annex G Radial Speed Error and Location 65
Annex H Examples of Ships at Various Aspect Angles 69
Annex I Examples of Ship Focus 70
References 72
List of acronyms 73

List of figures

Figure 1: Length histogram of analyzed ships according to the AIS data. 8
Figure 2: Aspect angle histogram of analyzed ships according to the AIS data. 9
Figure 3: Radial speed histogram of analyzed ships according to the AIS data. 9
Figure 4: Along-track speed histogram of analyzed ships according to the AIS data. 10
Figure 5: Scatter plot of radial speed for all scenes. 12
Figure 6: Histogram of radial speed error for all scenes. 13
Figure 7: Scatter plot of estimated ship aspect angle for all scenes. 16
Figure 8: Confidence measure of estimated ship aspect angle for all scenes. 17
Figure 9: Histogram of estimated aspect angle errors for all scenes. 17
Figure 10: Along-track speed estimation error for 99 ships that have $M > 0.4$ and $V_r > 1$ m/s. 19
Figure 11: Same as Figure 10, but for the 41 ships that are closest to range travelling. 19
Figure 12: Same as Figure 10, but for the 58 ships that are closest to azimuth travelling. 20
Figure 13: Along-track speed estimation error for the 99 ships of Figure 10, but using the map-drift algorithm. 20
Figure 14: Same as Figure 13, but for the 41 ships that are closest to range travelling. 21
Figure 15: Same as Figure 13, but for the 58 ships that are closest to azimuth travelling. 21
Figure 16: Histogram of relative ship length errors for nominally range travelling ships. 23
Figure 17: Histogram of relative ship length errors for nominally azimuth travelling ships. 23
Figure 18: Plot of relative ship length errors as a function of estimated aspect angle. 24
Figure 19: Power envelope for an azimuth travelling ship. 24
Figure 20: Power envelope for a range travelling ship. 25
Figure 21: Power envelope for the Resolute transponder. 26
Figure 22: Residual Doppler history for the Resolute transponder. 26
Figure 23: Residual range cell migration for the Resolute transponder. 27
Figure 24: Over-sampled image of the Resolute transponder; over-sampling factors are 8 in azimuth and 4 in range. 27
Figure 25: Azimuth PTR for the Resolute transponder. 28
Figure 26: Incidence angle histogram of analyzed ships 30
Figure 27: RCS as a function of ship length for various ship incidence angles. 30
Figure 28: RCS as a function of ship length for various ship aspect angles 31

Figure 29: RCS and σ° variations as a function of relative look bandwidth for the Resolute transponder. 33

Figure 30: RCS and σ° variations as a function of relative look bandwidth for D1S16, an 85 m long ship 34

Figure 31: RCS and σ° variations as a function of relative look bandwidth for D1S33, a 248 m long ship. 34

Figure 32: Histogram of differences between high- and low-resolution σ° estimates; calibration constants are from high- and low-resolution Resolute transponder images. 36

Figure 33: Differences between high- and low resolution σ° estimates as a function of σ°; calibration constants are from high- and low-resolution Resolute transponder images. 36

Figure 34: Power spectral density estimates for ocean before focusing: a) clutter-dominated case (D3S11) with σ° = –17 dB; and b) noise-dominated case (D7S2) with σ° = –24 dB. 37

Figure 35: Ship RCS and σ° variations as a function of relative look bandwidth for D7S2, a 117 m long ship. 37

Figure 36: Histogram of differences between high- and low-resolution ship RCS estimates; calibration constants are from high- and low-resolution Resolute transponder images. 38

Figure 37: Histogram of differences between ship RCS estimates from two symmetrical azimuth looks. 38

Figure 38: σ° map for Scene 1. 41

Figure 39: σ° map for Scene 2. 42

Figure 40: σ° map for Scene 3. 42

Figure 41: σ° map for Scene 4. 43

Figure 42: σ° map for Scene 5. 43

Figure 43: σ° map for Scene 6. 44

Figure 44: σ° map for Scene 7. 44

Figure 45: CDC map for Scene 1. 45

Figure 46: CDC map for Scene 2. 46

Figure 47: CDC map for Scene 3. 46

Figure 48: CDC map for Scene 4. 47

Figure 49: CDC map for Scene 5. 47

Figure 50: CDC map for Scene 6. 48

Figure 51: CDC map for Scene 7. 48

Figure 52: Along-track variation of CDC for several adjacent range bins for Scene 1. 49
Figure 53: Along-track variation of CDC for several adjacent range bins for Scene 2. 50
Figure 54: Along-track variation of CDC for several adjacent range bins for Scene 3. 50
Figure 55: Along-track variation of CDC for several adjacent range bins for Scene 4. 51
Figure 56: Along-track variation of CDC for several adjacent range bins for Scene 5. 51
Figure 57: Along-track variation of CDC for several adjacent range bins for Scene 6. 52
Figure 58: Along-track variation of CDC for several adjacent range bins for Scene 7. 52
Figure 59: D5S19, the 34 m long tug boat “AHT Braveheart”, seen here towing a large barge, is the smallest ship in the data set. 53
Figure 60: D7S1, the 63 m long freighter “Germa” is one of the smallest ships in the data set. 53
Figure 61: D6S1, the 347 m long cargo ship “Chastine Maersk” is one of the largest ships in the data set. 54
Figure 62: D4S19, the 332 m long tanker “Neptune Glory” is one of the largest ships in the data set. 54
Figure 63: D6S27, a ship with a poor V_r estimate but a good DC estimate. 54
Figure 64: D7S34, a ship with a poor V_r estimate but a good DC estimate. 54
Figure 65: D7S8, a ship with a poor V_r estimate. 55
Figure 66: D6S5, the same ship as D7S8, but with a good V_r estimate. 55
Figure 67: D2S2, a slow moving ship with a 180° direction error. 55
Figure 68: D5S4, a slow moving ship with a 180° direction error. 55
Figure 69: D3S15, a ship with an incorrect aspect angle for no apparent reason. 56
Figure 70: D7S34, a ship with an incorrect aspect angle for no apparent reason. 56
Figure 71: Geolocation of ships predicted from AIS data and reported by CHASP for Scene 1. 57
Figure 72: Geolocation of ships predicted from AIS data and reported by CHASP for Scene 2. 58
Figure 73: Geolocation of ships predicted from AIS data and reported by CHASP for Scene 3. 58
Figure 74: Geolocation of ships predicted from AIS data and reported by CHASP for Scene 4. 59
Figure 75: Geolocation of ships predicted from AIS data and reported by CHASP for Scene 5. 59
Figure 76: Geolocation of ships predicted from AIS data and reported by CHASP for Scene 6. 60
Figure 77: Geolocation of ships predicted from AIS data and reported by CHASP for Scene 7. 60
Figure 78: Histogram of radial speed errors for Scene 1. 61
Figure 79: Histogram of radial speed errors for Scene 2. 62
Figure 80: Histogram of radial speed errors for Scene 3. 62

Figure 81: Histogram of radial speed errors for Scene 4. 63
Figure 82: Histogram of radial speed errors for Scene 5. 63
Figure 83: Histogram of radial speed errors for Scene 6. 64
Figure 84: Histogram of radial speed errors for Scene 7. 64
Figure 85: Radial speed estimation error for Scene 1. 65
Figure 86: Radial speed estimation error for Scene 2. 66
Figure 87: Radial speed estimation error for Scene 3. 66
Figure 88: Radial speed estimation error for Scene 4. 67
Figure 89: Radial speed estimation error for Scene 5. 67
Figure 90: Radial speed estimation error for Scene 6. 68
Figure 91: Radial speed estimation error for Scene 7. 68
Figure 92: Image window with a ship at an aspect angle of 38°. 69
Figure 93: Image window with a ship at an aspect angle of 315°. 69
Figure 94: Image window with a ship at an aspect angle of 171°. 69
Figure 95: Image window with a ship at an aspect angle of 268°. 69
Figure 96: Ship D1S7: a) nominal parameters; b) adjusted DC and nominal DR; and c) adjusted parameters. 70
Figure 97: Ship D1S32: a) nominal parameters; b) adjusted DC and nominal DR; and c) adjusted parameters. 70
Figure 98: Ship D7S6: a) nominal parameters; b) adjusted DC and nominal DR; and c) adjusted parameters. 71

List of tables

Table 1: R-1 data over Strait of Dover used in this study. 7
Table 2: Parameters used for aspect angle estimation for the four example ships. 15
Table 3: Ship parameters for focus examples. 70

Acknowledgements

We thank John Wolfe and Dr. Ryan English (DRDC Ottawa) for helpful input concerning the analyzed data set and for valuable discussion and insight. We thank Dr. J.K.E. (Jake) Tunaley (Polar Epsilon R&D Manager) for his interest in and support of this work.

This page intentionally left blank.

1. Introduction

The Chip-based Adaptive SAR Processor (CHASP) was originally developed at Defence R&D Canada – Ottawa (DRDC Ottawa) to facilitate the precision processing of Environment Canada (EC) CV-580 C-band polarimetric airborne SAR data [2]. The initial purpose of CHASP was to improve the image data quality and to provide reliable data sets for downstream analysis and algorithm development that could be relevant to RADARSAT-2 (R-2) data processing. The EC CV-580 SAR operates under rather different conditions (e.g., geometry and platform speed) than RADARSAT-1 (R-1) or R-2 [3]. As a consequence, airborne SAR signals are subject to a significant Doppler shift and Doppler modulation in the case of moving vessels and/or vessels operating within a wave field. CHASP has been proven useful in reducing the adverse effects of vessel motion and producing better focused images of ships [3]. During its operation, CHASP extracts information concerning the target, the background clutter, and the relative ship motion. This extracted information is made available in the image header file as target and clutter attributes.

Further effort has been extended toward the processing and analysis of R-1 data. The principal goal of the present investigation was to determine which of the CHASP methods remain relevant in the case of R-1 input data, and which of the target attributes can be estimated by CHASP from R-1 data. As part of this effort, some additional functionality was added to CHASP and a separate, standalone program was developed to accept, reprocess, and analyze single look complex (SLC) data that may originate from a commercial SAR processor. However, it is very clear that range-compressed, azimuth-non-compressed SAR data (referred to henceforth as RC data) are by far more useful when dealing with moving targets. This is because the SAR front-end processing, up to the range compressed level, is lossless in the sense that no information acquired by the radar gets lost in the processing chain; only certain characteristics of the particular SAR instrument are removed. However, all further processing compromises the information embedded in the SAR signal to some degree. This further processing may be lossy, especially in the case of moving targets, and it always introduces some specific assumptions and characteristics of the particular SAR processor implementation. Working with RC data as the CHASP input requires a minimum of auxiliary information flow between the commercial SAR processor and CHASP. Required parameters include:

- The pulse repetition frequency (PRF) and sampling frequency (FS);
- The slant range of the first sample, i.e., the near slant range (NSR);
- A satellite state vector (SV) and its epoch time within or very close to the scene of interest; and
- The pixel dimensions of the range compressed data.

Should only an SLC image be available rather than RC data, the interface between the commercial SAR processor and CHASP must include much more information, most notably the applied Doppler centroid (DC) and Doppler rate (DR) throughout the image, the spectral bandwidth, and any shaping (i.e., data window) parameters. Furthermore, some level of detail concerning the particular implementation of SAR signal compression would be beneficial.

The main purpose of the work is to identify methods which have been developed in CHASP and determine which are applicable to R-1 processing of moving ship targets. In particular, CHASP algorithms have been applied to a statistically significant R-1 Fine mode data set that was acquired over the Straits of Dover in early 2005, and for which ship validation data acquired via AISLive is available [4].

This document is structured as follows: Section 2 describes the data processing procedures; Section 3 discusses the available validation data; and Section 4 presents processing results in the context of the available validation data. The conclusions of the study are presented in Section 5. Several analysis plots for each scene and examples of many ships are relegated to the Annexes.

2. Data processing

2.1 Added CHASP functionality

In order to carry out this analysis, new functionality has been added to CHASP itself or developed as additional standalone programs.

One of the new utilities is a program that generates antenna position vectors for each SAR pulse instant, covering the whole scene of interest. The input is a single satellite state vector; the output is in the same format as used for EC CV-580 SAR images by processors such as CHASP. This utility makes it possible to precisely georeference R-1 data using CHASP, independent of any external proprietary software.

Another standalone utility was developed to calculate the "PRF/V" parameter for the slant range of interest and for the along-track time of interest. The "PRF/V" parameter is the key focusing parameter in CHASP. For airborne SARs, this parameter is made available through motion compensation pre-processing. For R-1, it is based on a precise geometry model, the available SV, and the estimated DC.

CHASP georeferencing functions have been upgraded so that proper georeferencing is achieved, even if the SAR is not zero-Doppler steered.

CHASP functions for scene DC estimation have been refined. The DC ambiguity is not estimated in CHASP since it is completely predictable for R-1. Therefore, an approximate DC value (within half the PRF) is set through the configuration file. This value is used internally for the purpose of DC ambiguity resolution, but the fractional part is refined. Since the presence of a vessel disturbs the DC estimator, some filtering of the local values is implemented using a rank filter and averaging. The latest version of CHASP provides both the clutter DC estimate and the target DC estimate as output results in the header file.

A slight modification of the radial speed estimator was made in order to take into account the clutter DC. This is necessary since R-1 is not zero-Doppler steered.

Oversampling has been implemented so that inter-look misregistration can be measured at sub-pixel levels.

Azimuth multi-looking has been upgraded so that an arbitrary number of looks with the desired bandwidth and overlap can be produced. These looks can be normalized in various ways.

Additional software was developed for purposes of testing and validating the CHASP algorithms. A standalone utility was developed to determine the expected image position of the target, given its geographical position. Also, all processing is automated by a script file. This allows very fast processing of many cases of known ships.

The final analysis and presentation of the results is done via a Matlab™ script.

2.2 Processing procedure

The complete processing procedure for a R-1 scene consists of the following steps:

- Front-end processing may be performed by any SAR processor and includes: conversion to floating point numerical format, application of the receiver gains and normalization by the replica power, in-phase/quadrature conditioning, and range compression. Radiometric correction is desirable, but not essential. The RC data must be made available in a flat raster format.
- An ASCII header file for the RC data is created in the EC CV-580 style. The header must have correct entries for the number of lines, number of samples, and for the NSR.
- A SV at the SAR acquisition time is obtained either from the SAR processor or by means of an orbital propagator.
- A standalone program is used to generate the series of SAR positions for each pulse interval. This program also generates the SAR velocity and acceleration at the same PRF. The output of this program is in the Matlab™ format and can be read directly by CHASP. This file is fondly known as the "PRF file" that is routinely used in EC CV-580 processing.
- Available validation data (in this case, from AIS) are used to form a list of geographical coordinates that will be analysed. At the same time, other attributes of the known ships are extracted into lists so that they can later be compared to values estimated from the SAR data.
- A shell script is used to automatically generate configuration files for processing each of the ships for which validation data are available. One configuration file is created for every ship in the list. The configuration file defines the image coordinates of the chip that will be processed by CHASP. The image coordinates are derived automatically from the known geographical coordinates. The script can be run separately for each ship, one at a time, or, alternatively, another, higher level shell script can be run to drive CHASP successively for all ships in the list. These scripts can be run unsupervised, or they can be run in an interactive mode. The interactive mode does not require or permit any input from the operator, but it displays the analysed image chip and allows the operator to stop or proceed with processing. This function is provided so that image chips containing multiple ships can be skipped or processed manually. In the automatic mode, CHASP will process the target of highest backscatter, which is not necessarily the desired vessel, and estimates of the clutter attributes could be incorrect.
- Finally, various processing results are collected into tables and compared to the available validation data. This comparison has also been automated by a script.

The main processing is streamlined by one script, which is easily tailored to suit the desired type of analysis. Currently the following functionality is included:

- Refinement of the clutter;
- Refinement of the "PRF/V" parameter;
- Formation of the "nominal" or "before" adaptive processing image;
- Estimation of the ship's DC, azimuth position, and radial speed;

- Formation of the “adjusted” or “after” image;
- Zooming, oversampling, and map-drift processing;
- Variation of the resolution, number of looks, and estimation of the radar cross section (RCS).

The duration of the processing procedure depends on the location of the ship in the image since file access time is an important factor. Typically, this procedure is completed automatically in half a minute on any computer that has been tested. An interactive procedure takes longer because some diagnostic plots and processed images are displayed. The analyst is then asked to continue or not. If the analyst interrupts further processing, they can modify the chip coordinates to avoid multiple targets or coastline, or improve target centering prior to repeating the processing. Depending on the situation, this can be time consuming. In an operational scenario, the ship of interest would be automatically detected and a window would be applied to zero-out everything outside the window in the image domain. This has not been implemented in the current processing procedure since it was judged that there are an adequate number of single targets in the available imagery for a reasonable statistical sample.

3. Data

3.1 RADARSAT-1

All R-1 data sets considered were acquired using the Fine beam mode, as per Table 1. Although data from several geographic sites were available, we focussed on the Dover cases since each scene contains relatively many ships. In total, 121 ships were analysed in the 7 Dover scenes.

Annexes A and B contain figures that provide an overview of the processed scenes. The figures were generated by running CHASP systematically in small tiles covering the entire scene. The extracted parameters are the radar reflectivity, σ°, and the local clutter Doppler centroid (CDC). The influence of ships on the ocean σ° and on CDC has been minimized. Therefore, the σ° and CDC maps should be representative of the background clutter only, excluding any ships that may be present in the analysed image chip.

Having a significantly higher backscatter, land is clearly recognised in the σ° maps. Coastlines disturb the CDC estimator, which is a well known effect. This is visible in the CDC maps, although some filtering is applied in CHASP to mitigate the effect. CDC varies systematically across the scene, with minor local fluctuations. On land, these fluctuations may be caused by non-uniformity in the land reflectivity (due to a high ocean-land contrast), but on the ocean, such non-uniformity appears to be insignificant (small disturbances due to the presence of ships are filtered out) and CDC variations may be attributed to sea surface motion (i.e., surface current). The CDC maps show qualitatively that there is a small bias in the ocean CDC relative to the land CDC. This bias may be positive (Figure 48) or negative (Figure 46). At the bottom of the CDC map for the Dover 7 scene (Figure 51) there is a larger region of inconsistent CDC that is probably caused by the very low ocean clutter in that region, as seen in the corresponding σ° map (Figure 44). This area is noise-dominated, which results in the poor CDC estimate.

Annex C contains several transects that illustrate the CDC bias on the ocean. The transects are along the azimuth direction at the same slant range for several adjacent slant range bins. In Figure 52 from Scene 1, no bias is evident. In Figure 53, which shows CDC variation at near range, there appears to be a bias. From these and other plots, it is apparent that the ocean CDC bias may amount to several percent of the PRF, which amounts, roughly, to up to ±50 Hz.

In the areas of ocean CDC bias, we expect the bias to propagate into the estimate of the DC offset of a ship, and to affect the estimate of the radial velocity. Even if the DC of a ship is correctly estimated, a positive bias of the surrounding CDC estimate, taken as a reference, would cause a negative bias in the estimate of the DC offset. This would translate into a positive bias of the radial velocity estimate. A more detailed analysis could be based on a physical model for the DC and would require use of a land-mask.

Table 1: R-1 data over Strait of Dover used in this study.

Scene	orbit	date	start time [UTC]	beam	centre incidence
1	48,187 descending	27-Jan-2005	06:03:03.425	F1	39.42°
2	48,280 ascending	02-Feb-2005	17:51:35.543	F5	46.83°
3	48,387 descending	10-Feb-2005	05:54:45.250	F5	46.62°
4	48,287 descending	03-Feb-2005	05:58:55.562	F3	43.59°
5	48,480 ascending	16-Feb-2005	17:43:15.914	F2	39.79°
6	48,623 ascending	26-Feb-2005	17:51:34.205	F5	46.83°
7	48,823 ascending	12-Mar-2005	17:43:12.925	F2	39.78°

3.2 AIS

AIS data obtained at about the same time as the satellite pass time via AISLive were used to initiate the analysis of known ships and to validate the analysis results. The following AIS-derived data were used:

- Vessel apparent latitude (accounting for the ship displacement due to its radial speed);
- Vessel apparent longitude (accounting for the displacement due to its radial speed);
- Vessel speed;
- Vessel radial speed;
- Vessel aspect angle or vessel heading relative to the R-1 look direction; and
- Vessel length.

The main attributes of the analysed vessels are presented in the following figures. The relevant attributes include: vessel length, relative heading or aspect angle, radial speed, and along-track speed. Each ship was uniquely identified in an authoritative ship database for validation of the AIS ship parameters. The distribution of the analyzed ships with respect to ship length is presented in Figure 1. The shortest among the analysed ships is the 34 m long tug boat “AHT

Braveheart". The longest two ships are the 347 m long cargo ship "Chastine Maersk", and the 332 m long tanker "Neptune Glory". These ships, along with a few other interesting cases, are shown in Annex D.

In these scenes, many ships have a similar course (i.e., they occupy the main shipping lanes along either side of the strait), hence there is not very much diversity in the aspect angle. This is illustrated in Figure 2. The aspect angle is defined in the surface plane clockwise from the look direction, such that 0° corresponds to moving along the look direction away from the nadir, and 90° corresponds to essentially anti-parallel to the ground track.

The directionality of ships in the Dover scenes is also reflected in the histogram of radial speeds and along-track speeds, as presented in Figure 3 and Figure 4, respectively.

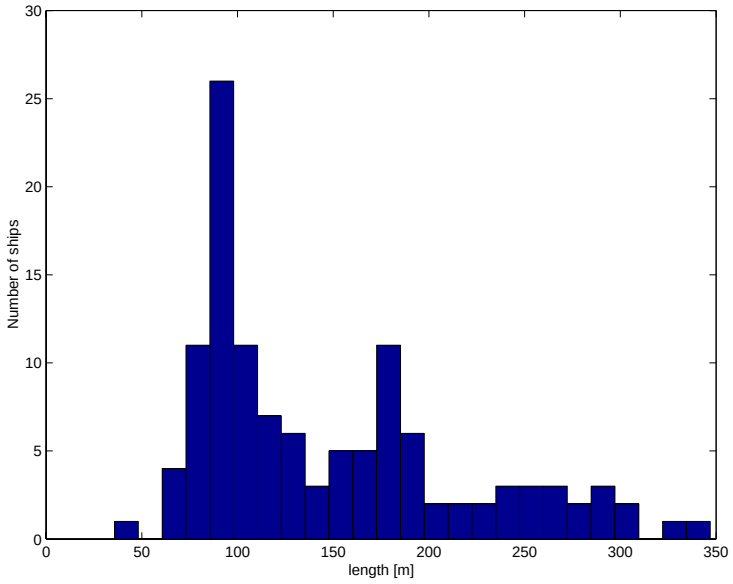

Figure 1: Length histogram of analyzed ships according to the AIS data.

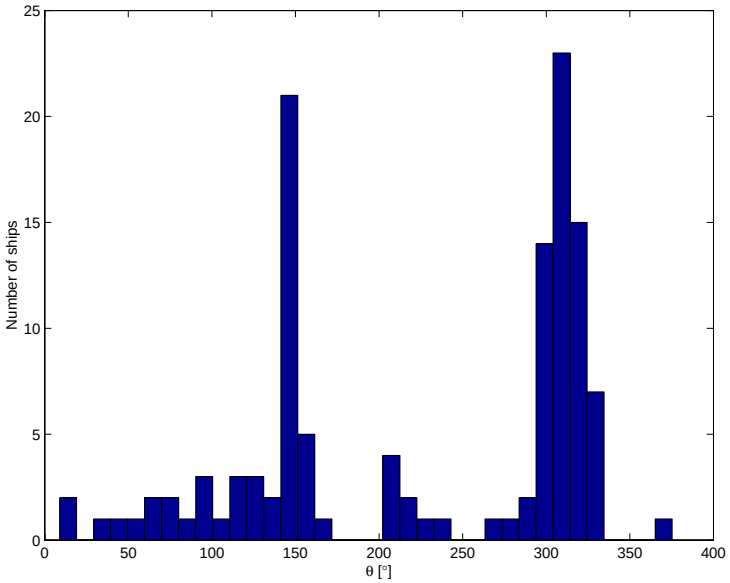

Figure 2: Aspect angle histogram of analyzed ships according to the AIS data.

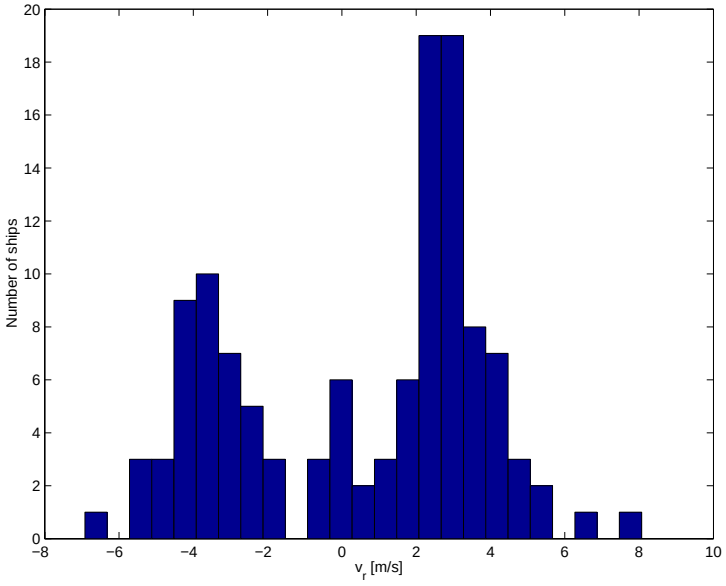

Figure 3: Radial speed histogram of analyzed ships according to the AIS data.

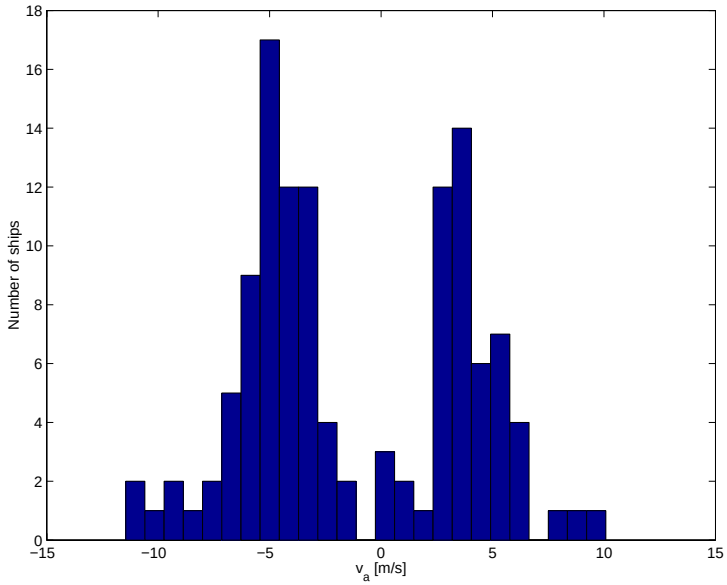

Figure 4: Along-track speed histogram of analyzed ships according to the AIS data.

4. Ship analysis results

4.1 Georeferencing

Apparent geographical coordinates, as predicted from AIS data, are compared to the geographical coordinates at which CHASP detected and georeferenced the ship. The agreement is good in all cases, as presented in Annex E. In some cases there seems to be a systematic offset. A small number of ships deviate more from the predicted positions. The exact cause is not known, though it could be related to vessel acceleration since only one AIS data point was available for validation purposes.

4.2 Radial speed

Radial speed estimation is closely related to the target DC offset. Several algorithms are implemented in CHASP, but only one has been used to complete the following analysis.

Radial speed estimates are derived in CHASP from three other estimates: the target beam-centre (acquisition) time (center of the power envelope in slow time before focusing); the target image position (upon focusing); and the static clutter DC (which is used as a speed reference).

Annex F shows the error distribution for the seven scenes considered, while Annex G shows the positions of the analysed ships with the estimation error colour coded; warmer colours represent positive errors in radial speed, while colder colours represent negative errors.

For Scene 1, the error is centred on zero, which agrees with the fact that the CDC is not biased, as illustrated by Figure 45 and by the transects shown in Figure 52. For Scene 2, the estimates are biased downward, which may be explained by a negative CDC bias, which is visible in Figure 46 and, more clearly, in Figure 53. Scene 3 has a positive bias, both in the radial speed error and in the CDC (Figure 54); however, there are several outliers. The situation is similar in Scene 4. There is no evidence of bias in Scene 5, nor in the speed estimates, nor in CDC, as shown in Figure 56. For Scene 6, the CDC estimates have a larger variation, as illustrated by Figure 57. This may be the reason for the larger variance of the estimation error. There is also one obvious outlier. In Scene 7 there are also areas with larger CDC variations, which may be responsible for a higher estimation error. There is one particular area, at the bottom of Figure 51, where the CDC fluctuations are exceptionally high, as also visible in Figure 58. This region is characterized by a low ocean clutter, as is evident in Figure 44; the region in question appears to be noise dominated. Two large outliers are evident exactly in that region (see Figure 91); the HH ocean clutter is too low and SAR signal is noise dominated, preventing accurate CDC estimation. Availability of a VV polarization channel (having a higher clutter level) would improve the speed estimation in this case.

All of these examples show that it is necessary to have good DC estimators and to account for any possible CDC bias. In all cases only the local CDC estimate, obtained immediately after range compression, are used. A more robust method would involve a physical model and global fitting (i.e., spatial diversity) via well proven algorithms that are available in the literature. An

additional modification could be based on landmasking to mitigate the influence of ocean surface movements on the CDC estimate.

Figure 5 shows the radial speed scatter plot for all ships in all scenes, while Figure 6 shows the histogram of the estimation errors. Both plots represent the estimation accuracy over all scenes, some with and some without a CDC bias that remains unaccounted for. Two of the three outliers are attributed to bad CDC estimates in a portion of Scene 7, while a third outlier is most likely caused by a similar condition in Scene 6. A more detailed investigation shows that all three ships are well focused with no visible azimuth ambiguities, suggesting that their own DC has been appropriately estimated. These cases are also included in Annex D. One of the ships is the 175 m long passenger ship "European Seaway" on the Dover-Calais-Dover line. The same ship is present and analysed in another scene on a different date. Its speed and direction were almost identical, but the radial speed was well-estimated in this case (with an error of 0.02 m/s).

The radial speed accuracy critically depends on the accuracy of the target position estimate, which in turn depends on the signal-to-clutter ratio and on the degree of fluctuation in the ship response. The ship length is known for 120 of the 121 analysed ships; only one of them is shorter than 50 m in length. The radial speeds of the four smallest ships were estimated quite well (errors of 1.1673 m/s, 0.4214 m/s, –0.6014 m/s, and 0.2417 m/s). A systematic relationship has not been found between the size of the ship and the estimation accuracy in this data set.

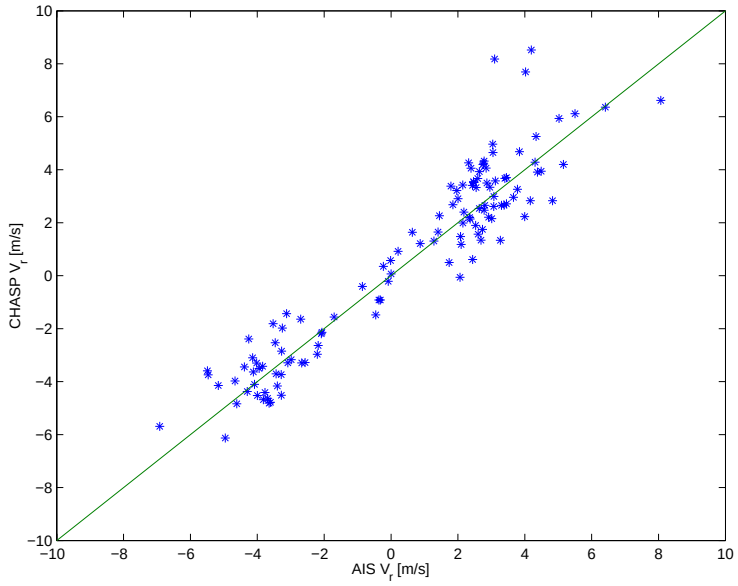

Figure 5: Scatter plot of radial speed for all scenes.

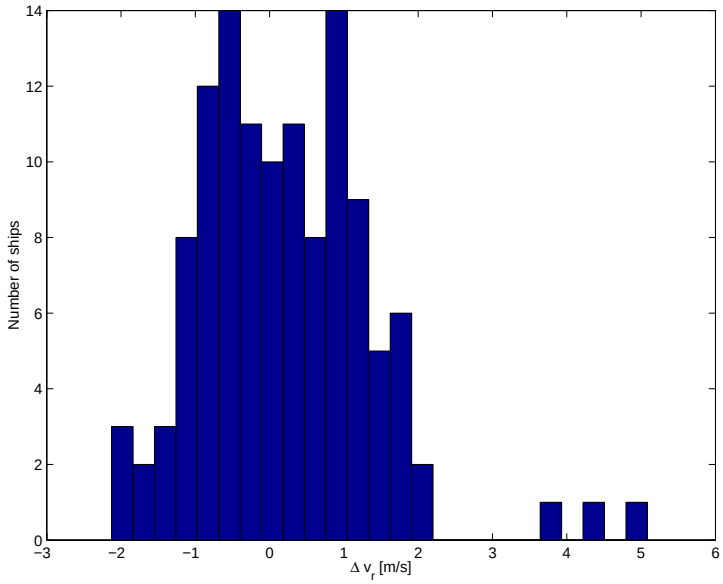

Figure 6: Histogram of radial speed error for all scenes.

4.3 Aspect angle

Aspect angle, or relative heading, is an important parameter because it can be used to estimate the target absolute heading and speed, given an estimate of the target radial speed. Furthermore, ship signatures depend on the ship orientation and ship RCS can, possibly, also be related to the aspect angle. Therefore, estimating the aspect angle is important and it is equally important to understand the accuracy that is achievable.

CHASP provides a rough estimate of the target aspect angle. The estimate is based on the size of a rectangular window that bounds the target. This window is defined as a rectangle containing the point of maximum illumination and adequately extending in range and in azimuth to capture the majority of the energy backscattered by the target. This window is estimated by a very simple procedure. Starting from the single brightest point in the ship signature, the window region is iteratively enlarged by alternately adding the next row and column until further addition does not contribute significantly to the observed target energy. When region growing stops, the range and azimuth bounds of the target are known in terms of the range and azimuth pixel spacings.

Annex H shows four representative examples of ships with different aspect angles. In each case, the window is centred at the brightest pixel and its sides are twice the length of the range and azimuth bounds. The pixel logarithmic intensity is colour-coded. The actual aspect angles of the illustrative ships are: 38°, 315°, 171°, and 268°, respectively. The first two ships are oriented approximately 45° from the look direction, but from different sides. The third ship is almost aligned with the look direction (and approaching the satellite), while the fourth is almost aligned with the ground track, and moving parallel to satellite. Visually, the windows created by the algorithm appear to be appropriate since the targets occupy roughly one-half of the window sizes, indicating that the region-growing algorithm has worked well.

Since the slant range spacing, local incidence angle, and azimuth pixel spacing are known, the range and azimuth bounds can also be expressed in physical units on the surface of the Earth. The ratio of the azimuth bound and ground range bound is used to calculate the off-look angle. The result is ambiguous, as demonstrated by the first two cases, for which this ratio is very similar. This ambiguity is resolved by using the sign of the quantity:

$$M_{ra} = \frac{\left\langle I(r,a)\left(r - \langle r \rangle\right)\left(a - \langle a \rangle\right)\right\rangle}{\langle I(r,a) \rangle}, \tag{1}$$

where r is range, a is azimuth, $I(r,a)$ is the image intensity, and $\langle \cdot \rangle$ denotes the spatial average within the target bounds.

For the 38° case, M_{ra} is negative; for the 315° case, it is positive. In a similar way, the positive quantities:

$$M_{rr} = \frac{\left\langle I(r,a)\left(r - \langle r \rangle\right)^2\right\rangle}{\langle I(r,a) \rangle}, \text{ and} \tag{2}$$

$$M_{aa} = \frac{\left\langle I(r,a)\left(a - \langle a \rangle\right)^2\right\rangle}{\langle I(r,a) \rangle} \tag{3}$$

may be evaluated. We will use the normalized quantity:

$$M = \frac{M_{ra}}{\sqrt{M_{rr} M_{aa}}} \tag{4}$$

as an aspect angle direction indicator.

At this point, another type of ambiguity must be resolved: the ship may be traveling in one of two opposite directions. The ambiguity between 38° and 218°, and between 315° and 135° may be resolved by using the estimated radial speed, which is positive in both of these cases, but would have to be negative for the opposing aspect angles.

Range traveling ships are a special case that can be processed according to the same rules. The problem here is that the ratio of the azimuth and range bounds cannot be zero even for perfectly range traveling ships because of their finite width. Therefore, there is always a systematic error in the aspect angle estimate for this ship orientation. The third ship has a positive M_{ra} value and a negative estimated radial speed, so its aspect angle is also uniquely determined.

Table 2: Parameters used for aspect angle estimation for the four example ships.

AIS aspect angle	Azimuth pixels	Range pixels	M	CHASP V_r [m/s]	CHASP aspect angle
38°	23	21	–0.887	4.28	43°
315°	26	21	0.951	4.96	316°
171°	8	29	0.796	–4.15	168°
268°	50	6	0.224	–0.22	99°

Azimuth traveling ships differ from all other cases in two ways. First, their image is always elongated in azimuth and their image azimuth bounds are always much longer than their physical length. Second, the 180° ambiguity cannot be resolved by using the radial speed component. Usually, the radial speed is close to zero and M is also close to zero. In most cases, the aspect angle is accurately estimated to within the 180° ambiguity.

Table 2 summarizes the factors that are used for aspect angle estimation for the four examples of Annex H. The actual length of the first three ships is around 200 m. The fourth ship is only 78 m long, but it appears to be stretched in azimuth.

The aspect angle estimation accuracy is illustrated by the scatter plot in Figure 7. Most of the ships appear to be close to the AIS-derived values. Three obviously wrong estimates are attributed to the 180° ambiguity, as explained above, because their aspect angles are close to 90° or 270°, and their estimation error is close to 180°. M is close to zero for all three of these cases. Therefore, M can be taken as an aspect angle confidence indicator. As shown in Figure 8, M is low for all aspect angles close to 90° or 270°, whether they are estimated correctly or not. True aspect angles of ships with this confidence measure lower than 0.25 are: 86°, 98°, 96°, 102°, 292°, 268°, and 77°.

Several ships show a larger value of M, but their aspect angle estimates are incorrect. Two of these cases exhibit the 180° ambiguity, although their aspect angle should be favourable for estimation (i.e., 301° and 211°) and their images are very clear. Both ships were moving slowly and the sign of the estimated radial speed appears to be incorrect. In one case, this is due to a CDC bias in the scene (a true radial speed of 2 m/s was estimated as –0.1 m/s), and in the other case, the ship was moving too slowly (its radial speed of – 0.2 m/s was estimated as 0.3 m/s). For ships that are not moving, obviously it is not possible to resolve the 180° ambiguity. Therefore, a better aspect angle confidence measure could be defined by also using the ship speed.

There are cases, however, that cannot be explained. In principle, an image of a ship can be skewed due to motion imparted on it by the underlying ocean wave field (primarily the pitching

and rolling motions). This effect may occur under certain sea state conditions and for certain ship lengths. It is also possible that the AIS data contained errors or that the ship location was in error; the geographic location accuracy in these cases appears to be lower than usual and some other parameters do not match as well as in most other cases.

To summarize, CHASP's simple algorithm is very fast and fairly accurate for the inherent level of processing complexity. If higher accuracy is required, then these estimates provide a good initial value for a more sophisticated algorithm that could refine them. For example, ship aspect angle and width-to-length ratio can be taken as two separate ship parameters, which can be jointly estimated by a pattern matching procedure. CHASP is mainly concerned with fast primary analysis; pattern matching of this nature would fit better into a secondary level of ship signature analysis.

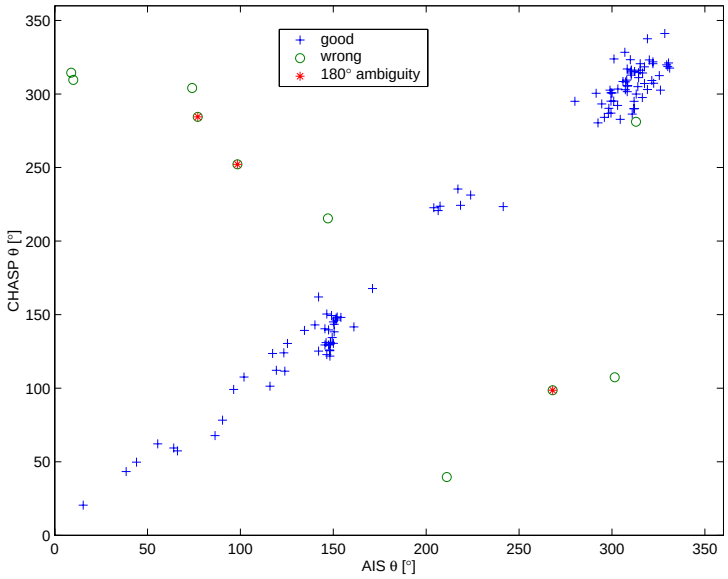

Figure 7: Scatter plot of estimated ship aspect angle for all scenes.

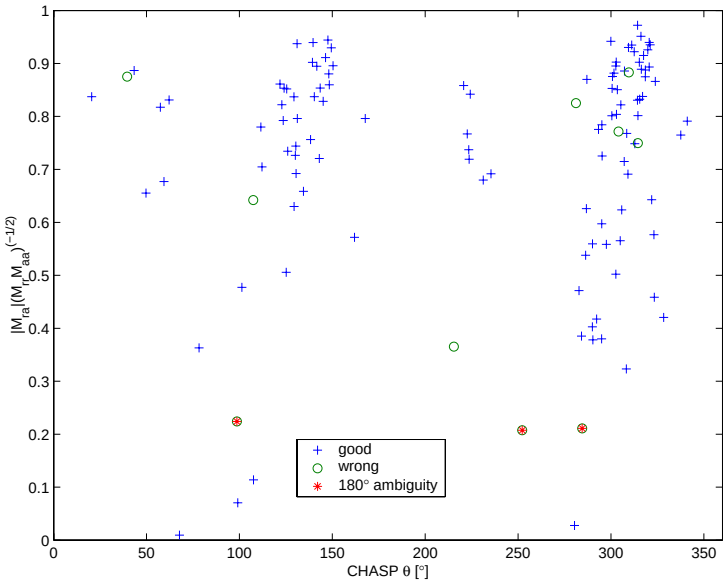

Figure 8: Confidence measure of estimated ship aspect angle for all scenes.

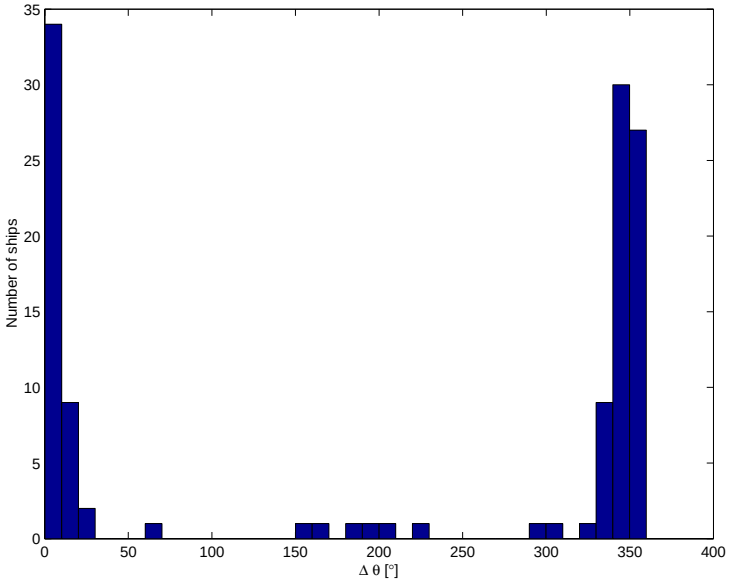

Figure 9: Histogram of estimated aspect angle errors for all scenes.

4.4 Along-track speed

Several algorithms for estimating along-track (i.e., azimuth) speed are implemented in CHASP. Most of them suffer from low sensitivity in the case of a spaceborne SAR. The most promising approach is to derive the along-track speed from the estimated radial speed, the estimated aspect angle, and the calculated incidence angle. For this method to work, some conditions must be met. Favourable conditions include high confidence in the aspect angle estimates and a high absolute value of the radial speed.

Figure 10 shows the histogram of the along-track speed estimation error for 99 out of 121 ships that have $M > 0.4$ and $V_r > 1$ m/s. The histogram includes two outliers with respect to the aspect angle. Similarly, Figure 11 is the histogram of the estimation error for 41 ships that satisfy the same conditions, but also have an estimated aspect angle within 45° of the look direction. Finally, Figure 12 is the histogram of the estimation error for the other 58 ships that have an estimated aspect angle within 45° of the track direction. It is apparent that large estimation errors are more likely to occur in the second case.

In comparison with these results, Figure 13, Figure 14, and Figure 15 are histograms produced from the map-drift algorithm (i.e., azimuth cross-correlation of sequential looks) for the same set of ships. Map-drift is performed on over-sampled images so that sub-pixel shifts can be detected. Over-sampling by a factor of 8 was used in azimuth. In some cases, the result was very accurate, with a high correlation coefficient between azimuth looks. However, many cases had large errors.

To summarize, the along-track speed cannot always be estimated with useful accuracy. Much better accuracy can be achieved for ships traveling with a large radial speed component than for ships traveling essentially along track. This accuracy can certainly be further improved by improving the accuracy of the radial component estimation (for example, by accounting for the CDC, as discussed previously) and by improving the accuracy of the ship aspect angle (for example by employing more sophisticated pattern matching algorithms, as also discussed previously). Ships that travel mostly in the along-track direction remain a problem, at least for the two methods considered here.

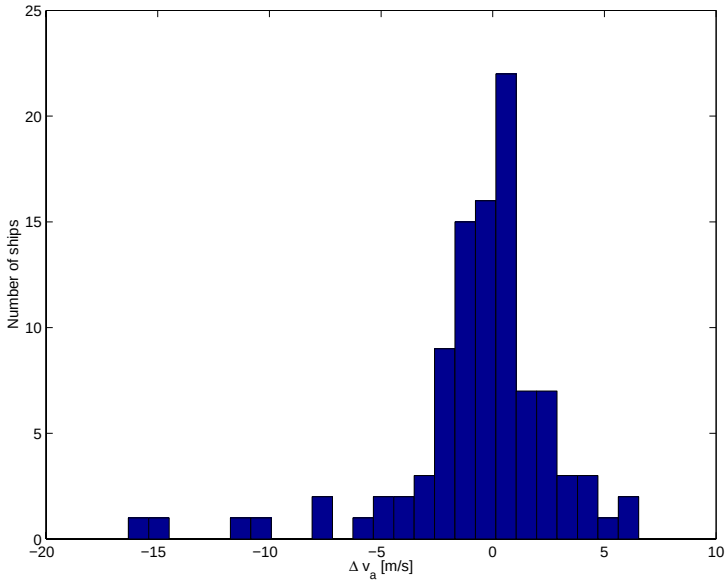

Figure 10: Along-track speed estimation error for 99 ships that have $M > 0.4$ *and* $V_r > 1$ *m/s.*

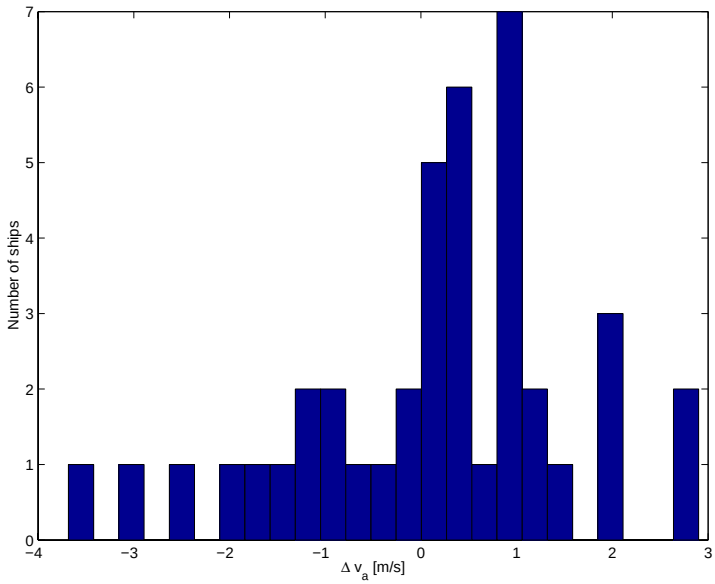

Figure 11: Same as Figure 10, but for the 41 ships that are closest to range travelling.

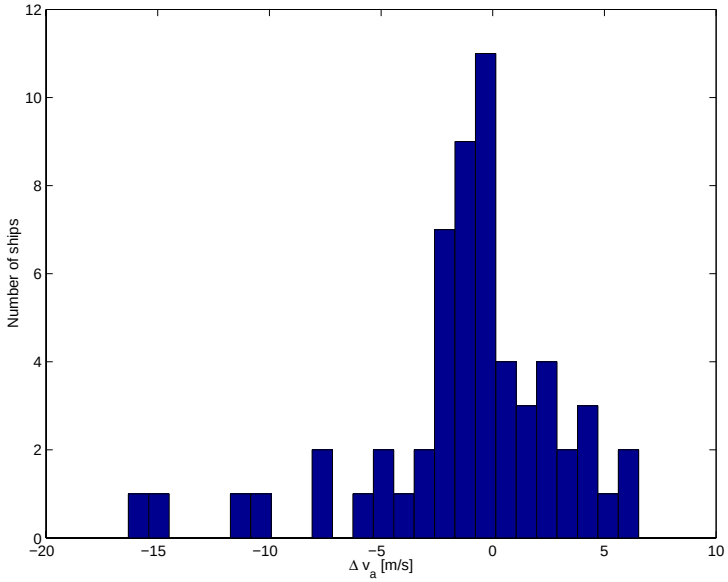

Figure 12: Same as Figure 10, but for the 58 ships that are closest to azimuth travelling.

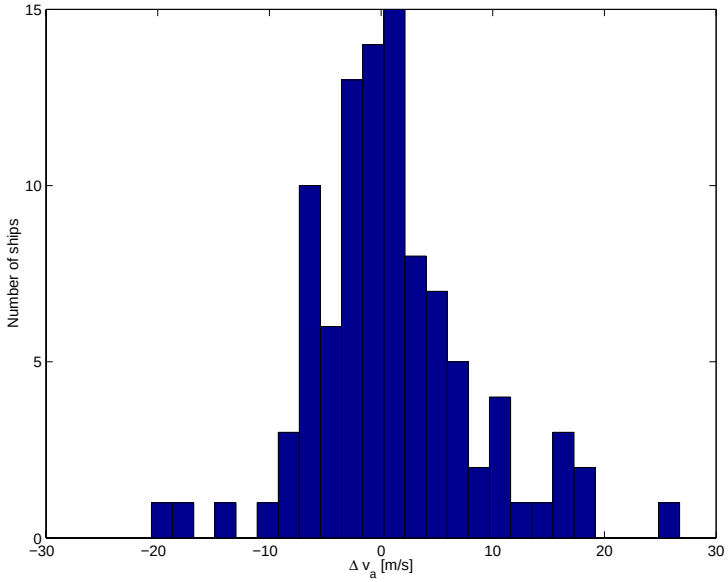

Figure 13: Along-track speed estimation error for the 99 ships of Figure 10, but using the map-drift algorithm.

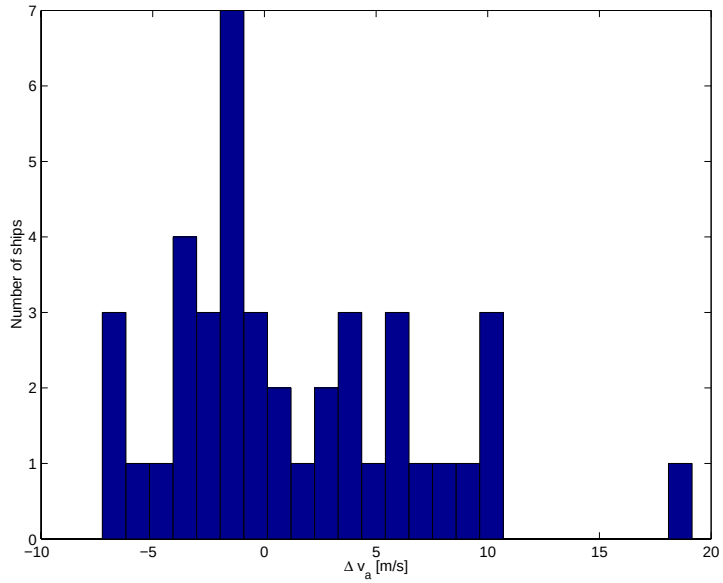

Figure 14: Same as Figure 13, but for the 41 ships that are closest to range travelling.

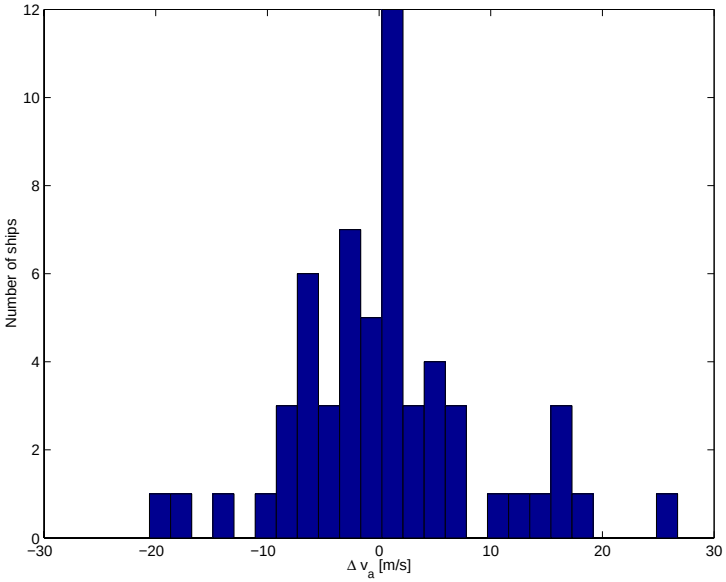

Figure 15: Same as Figure 13, but for the 58 ships that are closest to azimuth travelling.

4.5 Length

CHASP uses a simple algorithm for estimating ship bounds in terms of pixels in range and azimuth. This function is primarily intended for confining operations such as calculating orientation (i.e., aspect angle), center of mass, moments, range bins for Doppler history extraction (i.e., frequency tracking), contrast measurement (unless externally specified), etc. This simple algorithm can also be used as a rough estimate of the ship length under some conditions. Because of its intended purpose, it usually tends to overestimate the ship length.

For range travelling ships, in particular, this method can be successfully used as a rough estimator of ship length. Figure 16 shows the histogram of relative ship length errors for those ships that were within 45° of the look direction (i.e., nominally range travelling). Figure 17 shows the histogram of relative ship length errors for those ships that were within 45° of the ground track direction (i.e., nominally azimuth travelling). This is further emphasized when the relative ship length error is plotted as a function of the estimated ship aspect angle, as shown in Figure 18. We see that ships that are travelling closer to the satellite ground track (i.e., azimuth travelling) are more likely to have overestimated lengths. The largest relative error occurred for the case of a tug boat (39 m) towing a barge, since CHASP extracted the properties of the nearby barge rather than those of the ship itself.

The signature stretching of azimuth travelling ships may be caused by low coherence in the SAR response due to increased interference and due to motion such as pitching along the line of integration. This is illustrated by two ship examples of similar length (i.e., 155 m and 180 m), both taken from Scene 1. The first ship has an aspect angle of 96° (i.e., almost parallel to the ground track) and the second has an aspect angle of 378° (i.e., almost perpendicular to the first ship). The extracted power envelope in slow time (i.e., azimuth) for the two ships is shown in Figure 19 (azimuth travelling) and Figure 20 (range travelling), respectively. The power envelope of the ship has been separated from the clutter power by adaptive filtering. The shape of the envelope is very different in these cases and can be characterized by a modulation index: 0.79 for the azimuth travelling ship and 0.35 for the range travelling ship. The relative error of the length estimate is 1.4 for the azimuth travelling ship and 0.13 for the range travelling ship. Although this amounts to just a case study, this example has broader significance since it is fairly typical; as far as we know, this envelope modulation for azimuth travelling ships has not been previously observed. Note that both ships had essentially the same estimated RCS.

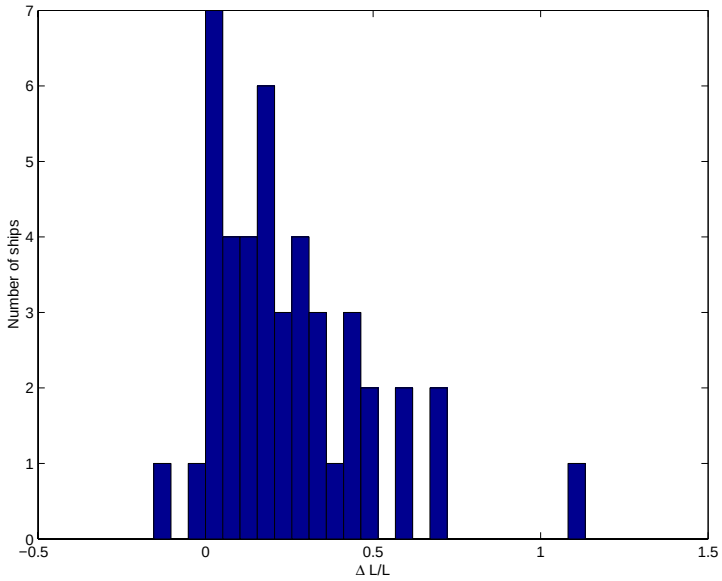

Figure 16: Histogram of relative ship length errors for nominally range travelling ships.

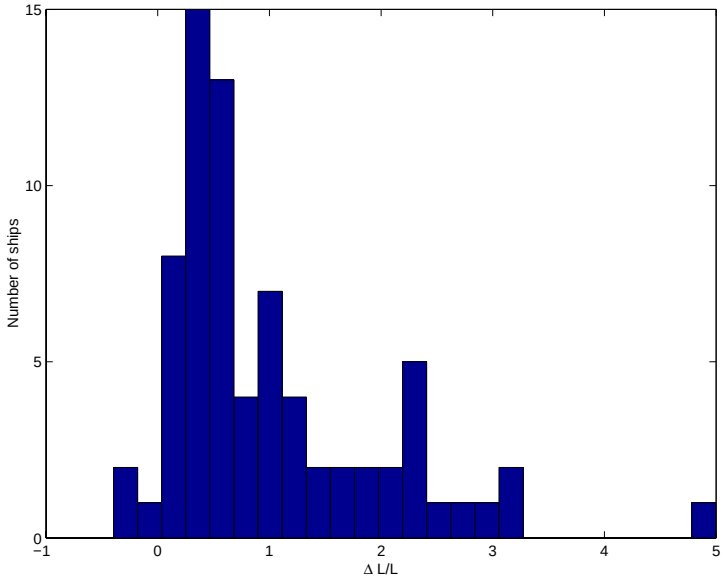

Figure 17: Histogram of relative ship length errors for nominally azimuth travelling ships.

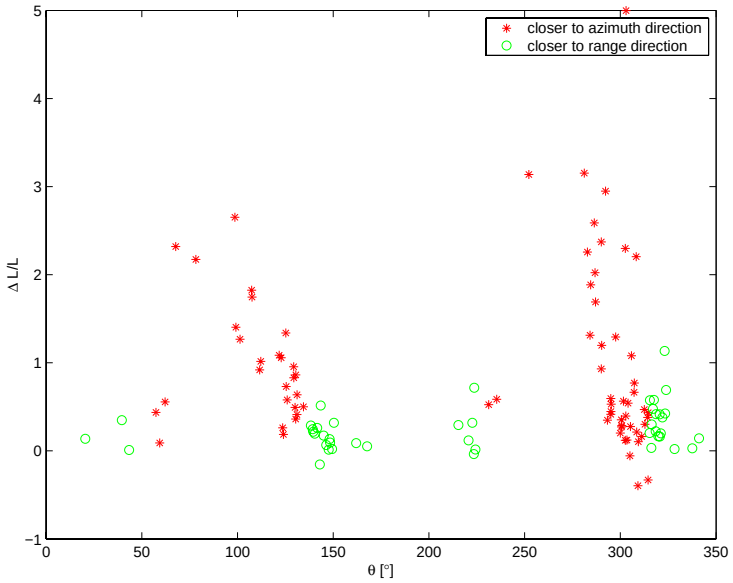

Figure 18: Plot of relative ship length errors as a function of estimated aspect angle.

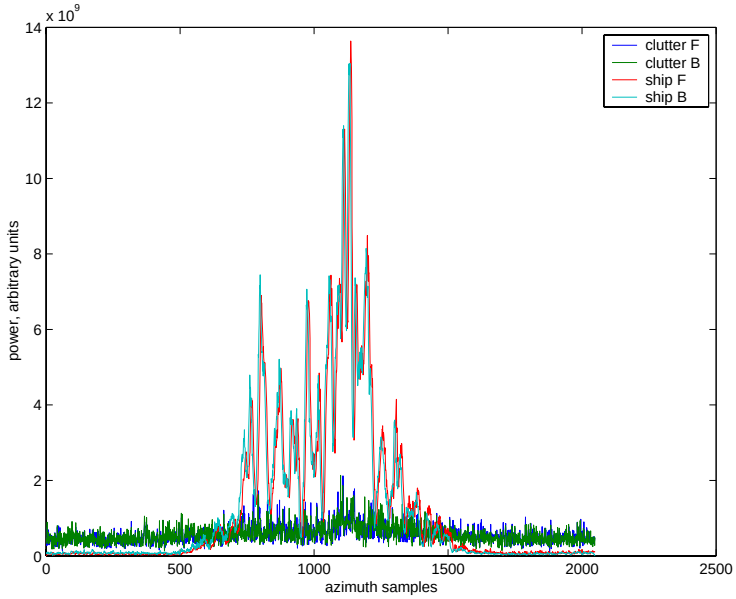

Figure 19: Power envelope for an azimuth travelling ship.

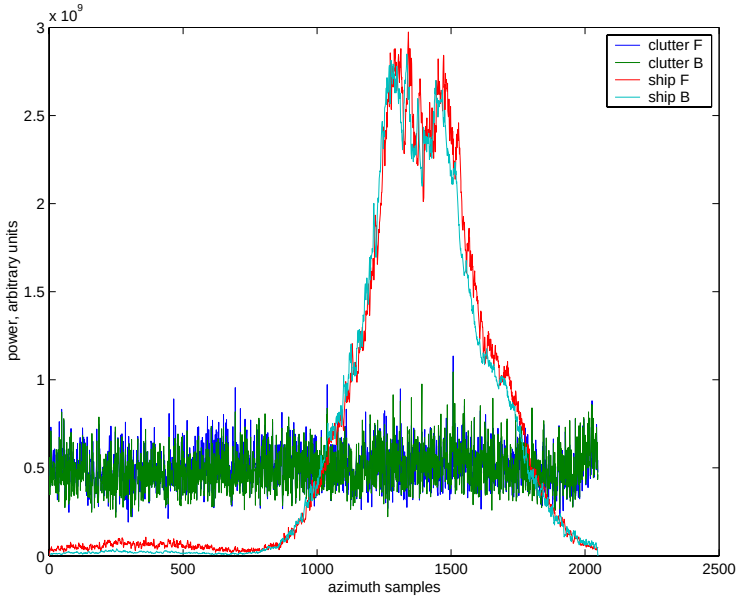

Figure 20: Power envelope for a range travelling ship.

4.6 Focus

The auto-focus capabilities of CHASP are first demonstrated on a Resolute transponder scene (i.e., a strong point target). One R-1 F4 scene over Resolute that contains the Canadian Space Agency (CSA) calibration transponder was used. The transponder is located at N74.746398° W95.001371° at an elevation of 68.0 m; it introduces a delay of 1.8 µs and has an RCS (at HH) of 55.51 dB-m^2. The transponder scene was processed to calibrate the processor, but the same data also serve to illustrate the focusing process.

Processing starts with an approximate DC value and with an approximate PRF/V value. The DC value is iteratively refined by the same algorithm used for ship processing (based on the difference between the image position and the raw position of the target response). The PRF/V value is refined by careful geometric calculations that include the DC offset (related to the SAR squint angle).

In the final iteration of the DC and PRF/V adjustments, Figure 21 shows the power envelope for the transponder response, Figure 22 shows the residual Doppler frequency upon applying the azimuth chirp, and Figure 23 shows the residual range cell migration. The same plots are produced for all ships and can be viewed by the analyst, but the procedure itself is automated.

Figure 24 shows the Resolute transponder point target response (PTR) with over-sampling by 8-times in azimuth and 4-times in range. An azimuth transect is shown in Figure 25 and is qualitatively judged to be essentially ideal.

It is important to point out that precise initial values are not needed (though they should be within PRF/2) and that the focusing procedure is fast and automatic.

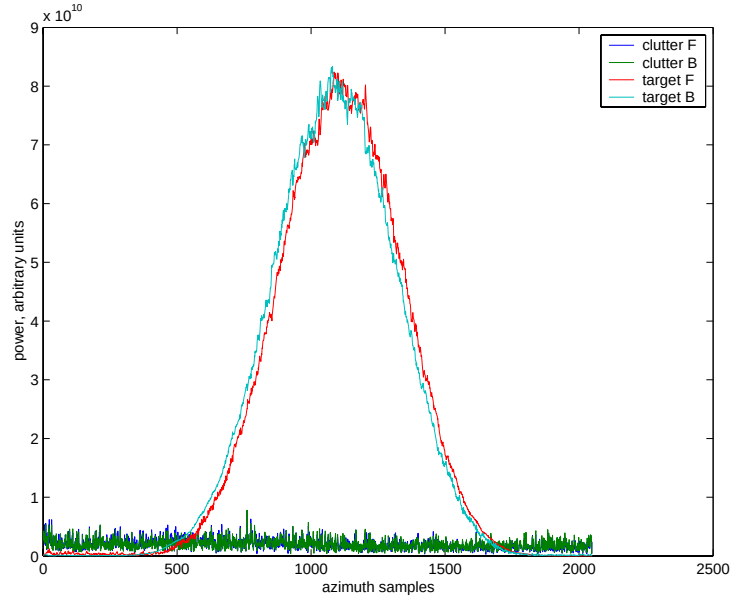

Figure 21: Power envelope for the Resolute transponder.

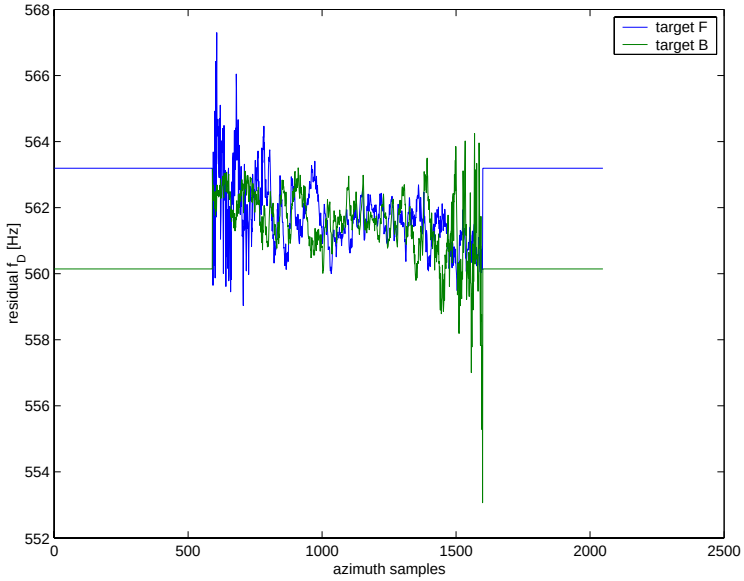

Figure 22: Residual Doppler history for the Resolute transponder.

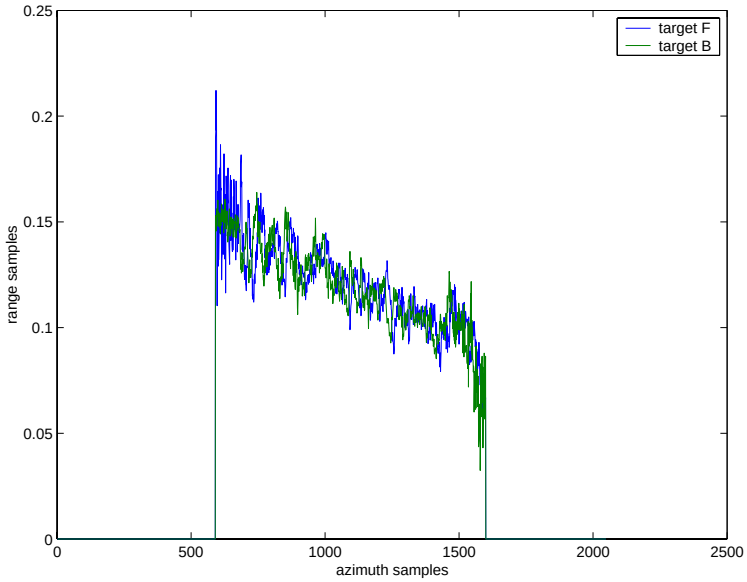

Figure 23: Residual range cell migration for the Resolute transponder.

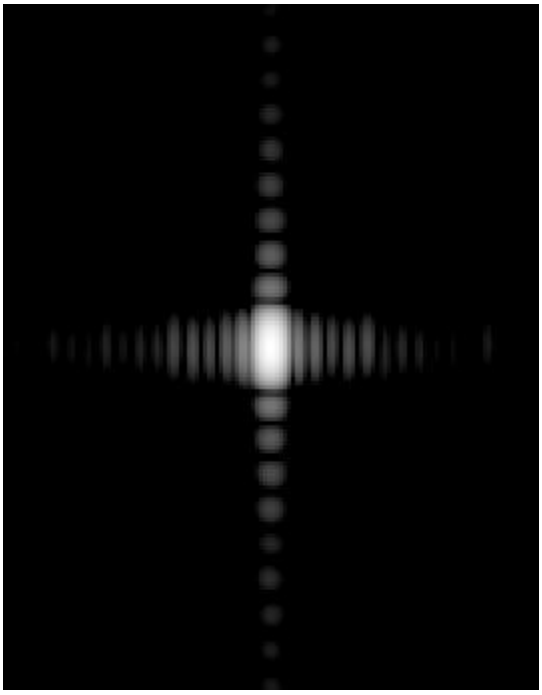

Figure 24: Over-sampled image of the Resolute transponder; over-sampling factors are 8 in azimuth and 4 in range.

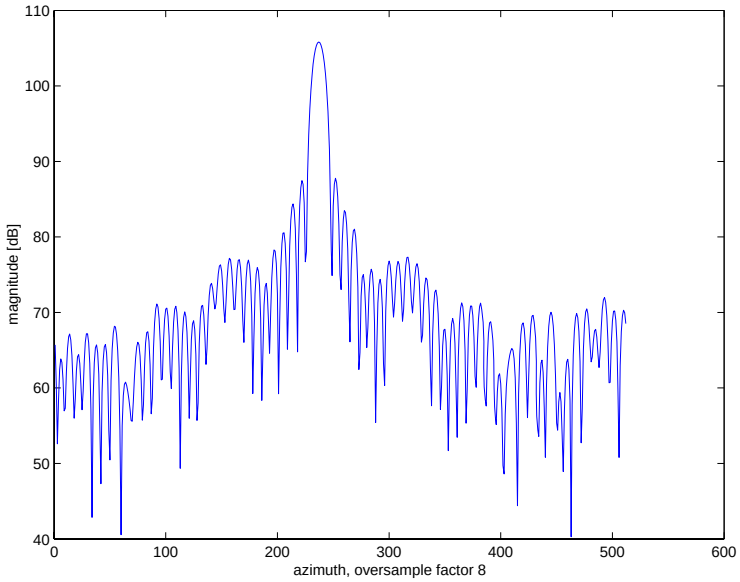

Figure 25: Azimuth PTR for the Resolute transponder.

The Resolute transponder example illustrates how focusing works for stationary targets. For ships, the DC is estimated in a similar way and focus improvements arise from DC adjustment, which removes ambiguities that may be present due to uncompensated ship radial speed. PRF/V depends negligibly on the speed in the along-track direction, though it may be affected by ship motion imparted by the underlying wave field. However, the effects of ship motion make no significant contribution to PRF/V and, therefore, no adjustments are applied (other than those related to geometry calculations). Some examples are shown in Annex I; it can be seen that the visual effects of the ship speed adjustment are marginal.

4.7 Radar cross section

CHASP includes algorithm for estimating the RCS of targets using the four corner method for clutter σ° estimation. This method is applied to all image chips with ships in an automated manner. It was first verified that there were no other ships within the analysis chip, a requirement for reliable σ° estimation. Two cases where eliminated from the analysis because other vessels lay within in the same chip.

All processing is done using a combination of a commercial SAR processor, used in a non-standard way (i.e., processing only up to the RC level) and CHASP (for focusing). Therefore, absolute calibration had to be carried out for this processing chain. The Resolute scene was processed using exactly the same processing chain (including all adaptive steps) as the Dover scenes with ships. Based on this processing, the absolute calibration constant for the processing chain was determined. This calibration constant, determined on an F4 scene, should also be valid for the Dover scenes, which were imaged with the F1, F2, F3, and F5 beams.

Figure 26 shows the histogram of incidence angles of ships in all Dover scenes. The first population is from the F1 and F2 scenes with a mean incidence angle for ships of 39.67°. The second population is from one F3 scene with a mean incidence angle for ships of 43.41°. The third population is from the F5 scenes with a mean incidence angle for ships of 46.71°.

In this context, we consider two empirical models for the ship RCS. Model A gives the ship RCS in metres-squared as [1]:

$$\sigma_A = 0.08L^{7/3}(0.78 + 0.11\theta) \tag{5}$$

where L is the ship length expressed in metres and θ is the incidence angle expressed in degrees. Model B gives the ship RCS in metres-squared as [4]:

$$\sigma = 1.25L^{1.98} \tag{6}$$

Both models were derived using R-1 images of known ships; Model B includes the ships that are being considered in this document.

Figure 27 shows CHASP estimates of the ship RCS as a function of ship length (plotted on a logarithmic scale). The straight lines are according to the empirical modes. Model A has been plotted for the three incidence angle populations noted above, representing different beams. Qualitatively, the model functions fit the actual measurements quite well. The three populations (with respect to the incidence angle) are shown in different colours.

Figure 28 shows the same information except that the ships have been divided into two groups depending on their nominal aspect angle. Qualitatively, there is no significant difference between the range travelling and azimuth travelling ships. For range travelling ships, CHASP estimates are, on average, 2.3 dB below Model A and 0.3 dB above Model B, with a standard deviation of 2.9 dB. For azimuth travelling ships, CHASP measurements are 1.3 dB below Model A and 1.3 dB above model B, with a 4.2 dB standard deviation. These observations have been made without resorting to any statistical tests as to whether there is a difference between the two sets.

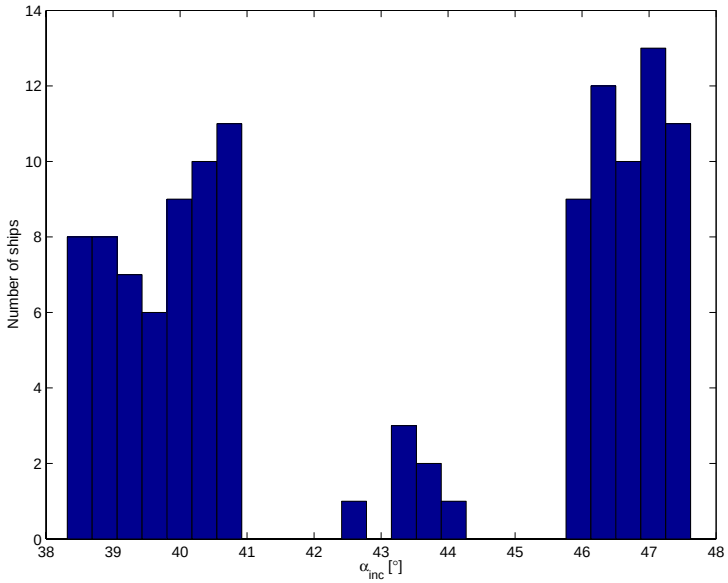

Figure 26: Incidence angle histogram of analyzed ships

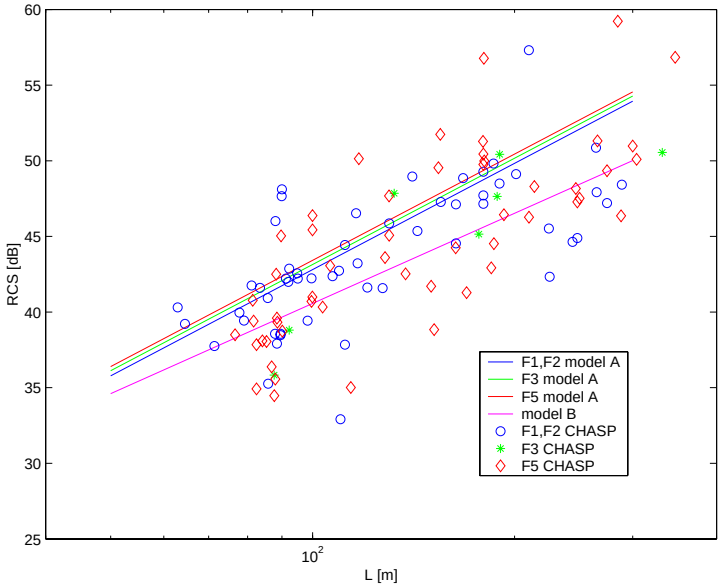

Figure 27: RCS as a function of ship length for various ship incidence angles.

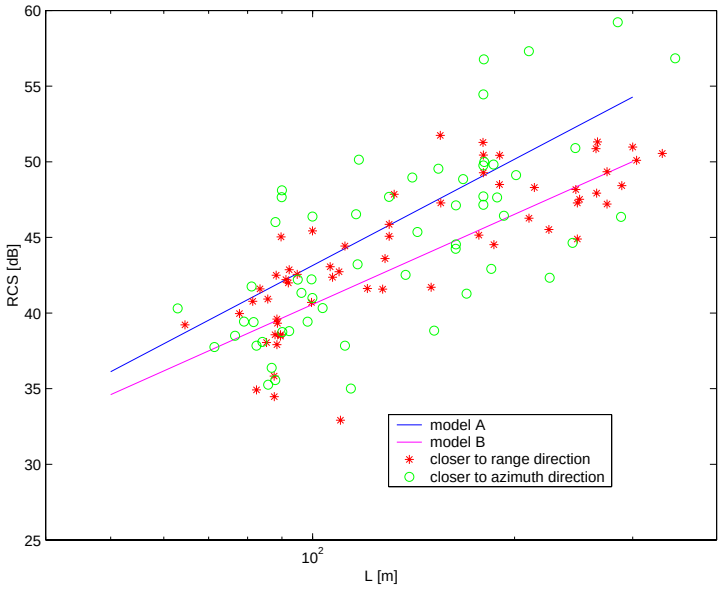

Figure 28: RCS as a function of ship length for various ship aspect angles.

CHASP supports multi-looking via windowing in the frequency domain, followed by incoherent look summation. A single look image is computed by applying a single frequency window $W(f)$ of bandwidth B to the signal $S(f)$, while multi-looking is achieved by applying a set of K shifted spectral windows $w(f - f_k)$ each of bandwidth $b < B$. Considering just one dimension (i.e., range or azimuth), the integrated response in the single look case is:

$$P_{SL} = \int |s_{SL}(t)|^2 \, dt = G \int W^2(f) |S(f)|^2 \, df \,, \tag{7}$$

and for the multi-looking case is:

$$P_{ML} = \int |s_{ML}(t)|^2 \, dt = \sum_k g_k \int w^2(f - f_k) |S(f)|^2 \, df \,, \tag{8}$$

where G and g_k are look weights, and the integration may be done either in the time (compressed) or the frequency domain. In practice, integration is done in the time domain around the target response, with integration limits usually depending on the resolution. Integration limits in the frequency domain are determined by B, b, and f_k.

Multi-looking can be performed in CHASP with several different normalization strategies that aim at preserving the background σ° value. The rationale for each choice is briefly described as follows.

First, when $S(f)$ is flat, i.e. $S(f) = S_0$ within the bandwidth B (as is the case in range frequency), integrated responses in the single look and multi-look case can be made equal by various choices of the weights g_k ; the simplest choice is:

$$1/G = \int W^2(f)df \tag{9}$$

and

$$1/g_k = 1/g = K\int w^2(f)df \tag{10}$$

This option is implemented and can be selected as "uniform weighting'" from the configuration file.

The second option is motivated by the fact that the azimuth spectral response is not flat, even in an ideal case such as a uniform background or a point target. The spectral response is then shaped by the antenna radiation pattern, with the addition of thermal noise. For a known azimuth antenna gain pattern and negligible thermal noise, there are again many solutions for g_k, which preserve the integrated response of a uniform scene (i.e., preserve σ°); one of these has been implemented in CHASP. However, it has not proven to be very useful based upon actual σ° and RCS measurements since it did not provide invariant σ° estimates when changing the look bandwidth. Presumably this is because the additive thermal noise is not negligible.

The third option is based on the following approximations:

$$P_{SL} \approx \Delta f \sum\nolimits_n W^2(f_n)\left|S(f_n)\right|^2 \tag{11}$$

and

$$P_{ML} \approx \Delta f \sum\nolimits_k \sum\nolimits_n g_k w^2(f_n - f_k)\left|S(f_n)\right|^2 \tag{12}$$

where f_n are N uniformly spaced (at interval Δf) frequencies. If a large number of looks is used ($K \gg 1$), with significant overlap, then an over-determined system of equations:

$$\sum\nolimits_k g_k w^2(f_n - f_k) = W^2(f_n) \tag{13}$$

can be solved (in the least-squares sense) to allow $P_{ML} \approx P_{SL}$, independent of the true spectral density $\left|S(f)\right|^2$. With this choice, σ° is approximately preserved when the number of looks and

their bandwidth is changed and, similarly, the RCS remains approximately unaffected. This option is also implemented and can be configured by selecting "normalized'" weighting and by suitably choosing the look bandwidth b, look overlap f_{ov}, and the number of looks K, keeping in mind that:

$$B = Kb - (K-1) f_{ov}. \tag{14}$$

Multi-look normalization is first demonstrated for the Resolute transponder and then for several ships. Different numbers of looks were used (7, 9, 11, 13, 15, 17, 19, 22, 25, 29, 33, 37, and 47) with $f_{ov} = 0.75b$ in each case, so that $b = 4B/(K+3)$ and $f_{ov} = 3B/(K+3)$.

Figure 29 shows the estimated RCS and σ° variations as a function of the relative bandwidth (b/B) for the Resolute transponder. Similarly, Figure 30 shows the RCS and σ° results for an azimuth travelling 95 m long ship, while Figure 31 shows similar plots for a 248 m long ship that was travelling at an aspect angle of 308°. The trend in these results is always the same.

This result does not necessarily imply RCS insensitivity to SAR resolution in general. It simply shows how signal processing can manipulate signals acquired with a certain resolution and how the choice of the signal processing options could depend upon the application. This result also shows that various multi-looking strategies can affect RCS measurements; accurate interpretation of RCS requires knowledge of the implemented multi-looking method.

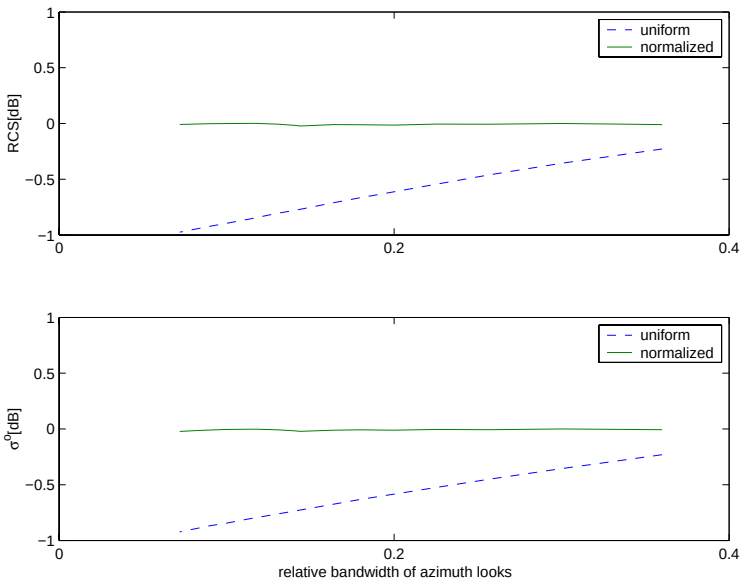

Figure 29: RCS and σ° variations as a function of relative look bandwidth for the Resolute transponder.

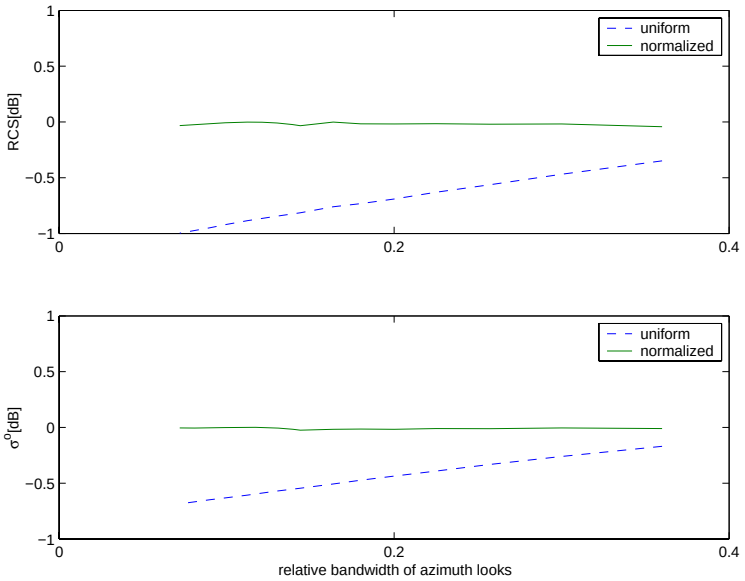

Figure 30: RCS and σ° variations as a function of relative look bandwidth for D1S16, an 85 m long ship

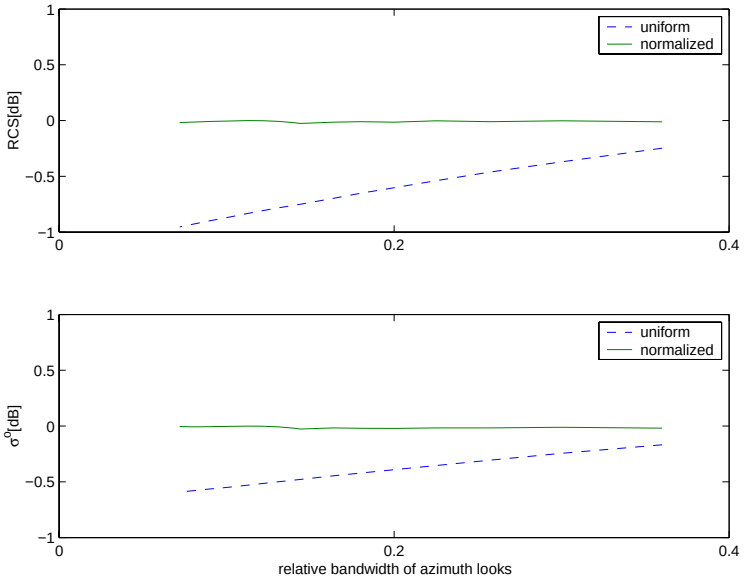

Figure 31: RCS and σ° variations as a function of relative look bandwidth for D1S33, a 248 m long ship.

In order to study RCS sensitivity to resolution, we repeated the processing using the same procedures, but with one-third of the previously processed Doppler bandwidth for both the Resolute transponder and Dover scenes. An implication of the change in processed Doppler bandwidth is that the calibration constant also changes. As a check, the estimated σ° for the Resolute scene was compared and found to be the same for the two processed bandwidths (i.e., resolutions).

On the other hand, it was found that σ° estimates for the Dover scenes were not identical at the two resolutions. The difference in σ° estimates is represented in histogram form in Figure 32 and by the plot in Figure 33. The plot shows larger discrepancies between the two σ° estimates for weaker clutter conditions, while the estimates tend to agree for stronger clutter conditions. Higher σ° estimates for the higher processed bandwidth case are expected for noise-dominated, that is, low-clutter conditions, because noise has a broader bandwidth than the signal used for calibration.

Meanwhile, it is possible to confirm by a simple spectral analysis test, that the difference in the two σ° estimates depends, indeed, on whether the clutter or the noise is dominant. An example of the two cases is presented in Figure 34. In this plot, the power spectral density before focusing is shown for the parts of the image chip that contain only ocean backscatter. The two cases are plotted with the same vertical scale (although the absolute calibration constant has not been used in either case). In the first case (D3S11), there is evidence of antenna pattern-shaped clutter, the σ° estimate is –17 dB, and there is only 0.09 dB difference between the high-resolution and low-resolution σ° estimates. In the second case (D7S2), the noise floor is dominant and there is little evidence of the antenna pattern-shaped clutter, the σ° estimate is –24 dB, and there is 0.94 dB difference between the high-resolution and low-resolution σ° estimates.

There is one other feature of the noise dominated chips that is worth noting. Figure 35 shows the variations of σ° and RCS estimates as a function of the relative look bandwidth in multi-look imagery. Unlike the cases considered previously (i.e., clutter dominated), σ° remains essentially constant for uniform weighting. On the other hand, the ship RCS appears to vary in a systematic way due to the uniform weighting of the azimuth looks.

Ship RCS estimates have more variance than the σ° estimates when the processed Doppler bandwidth changes. This is illustrated by Figure 36. These RCS measurements were made using the same technique, first in the high-resolution imagery and then in the low-resolution imagery.

Finally, an experiment was run to investigate ship RCS variability. The same bandwidth was processed twice, but from opposite sides of the DC representing two independent looks. Calibration of each look was done using the Resolute transponder. As expected, there was not any difference in the calibration constant since the azimuth antenna gain pattern is symmetric. Figure 37 shows that the histogram of the RCS difference between the two looks is symmetrical about the DC. There are noticeable differences that are larger than the differences between the high resolution and low resolution images.

These processing experiments have not revealed any systematic changes in ship RCS with resolution. However, the variations observed are not surprising, given the complexity of ship structures, the fact of ship motion, and the associated fading processes.

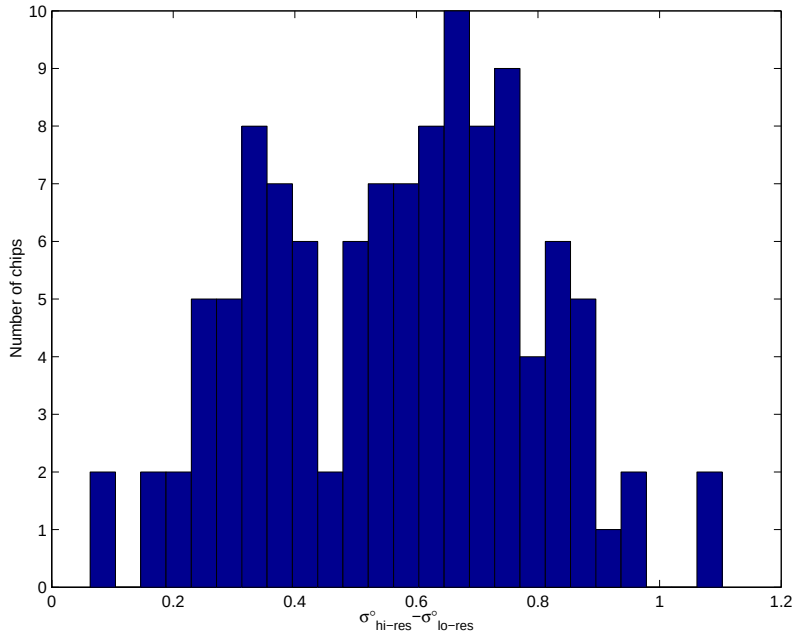

Figure 32: Histogram of differences between high- and low-resolution σ° estimates; calibration constants are from high- and low-resolution Resolute transponder images.

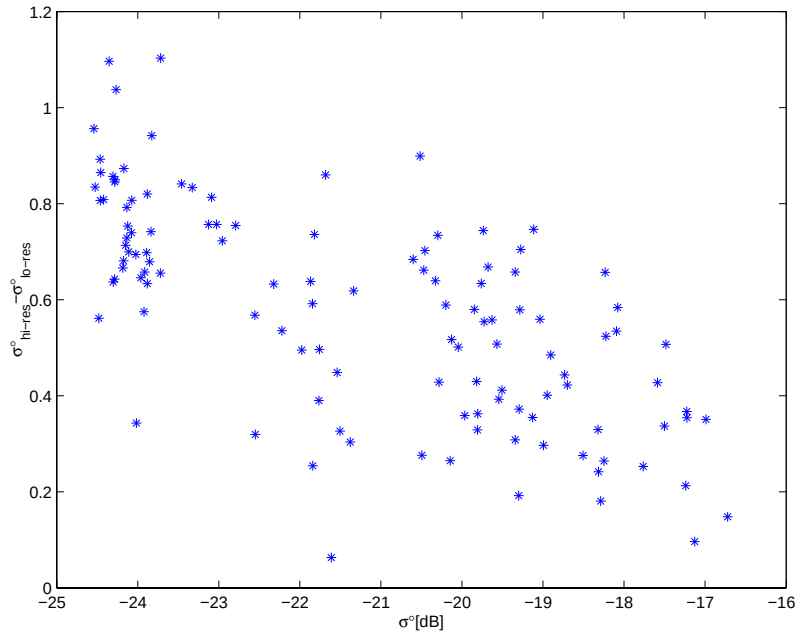

Figure 33: Differences between high- and low resolution σ° estimates as a function of σ°; calibration constants are from high- and low-resolution Resolute transponder images.

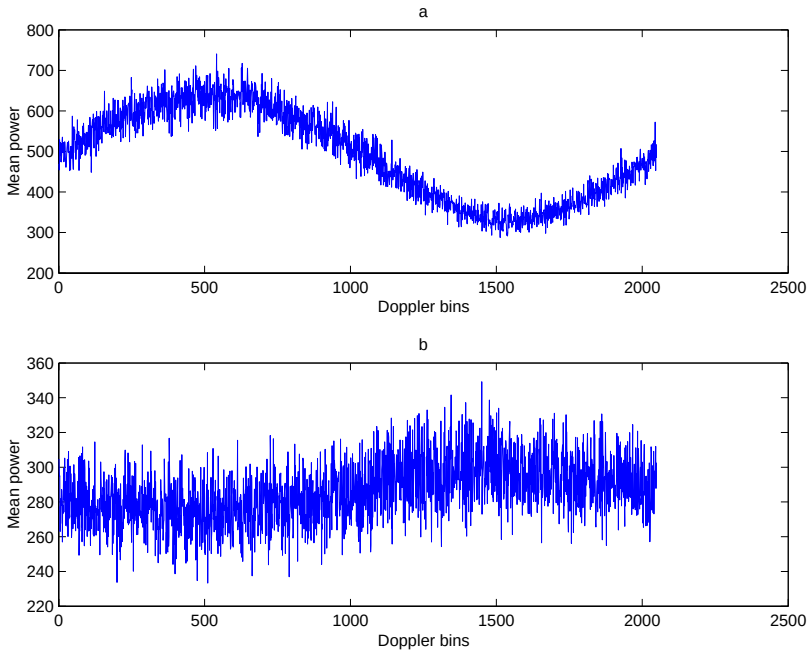

Figure 34: Power spectral density estimates for ocean before focusing: a) clutter-dominated case (D3S11) with σ° = –17 dB; and b) noise-dominated case (D7S2) with σ° = –24 dB.

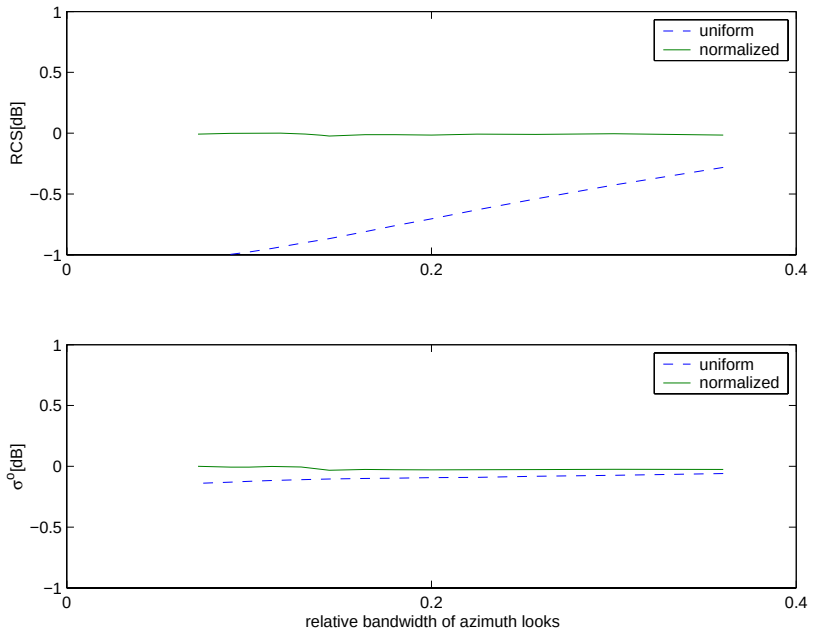

Figure 35: Ship RCS and σ° variations as a function of relative look bandwidth for D7S2, a 117 m long ship.

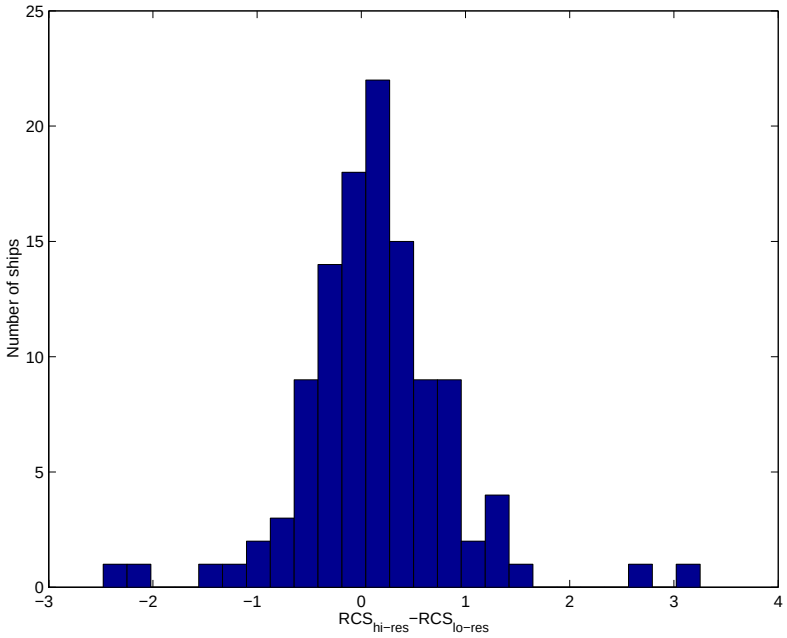

Figure 36: Histogram of differences between high- and low-resolution ship RCS estimates; calibration constants are from high- and low-resolution Resolute transponder images.

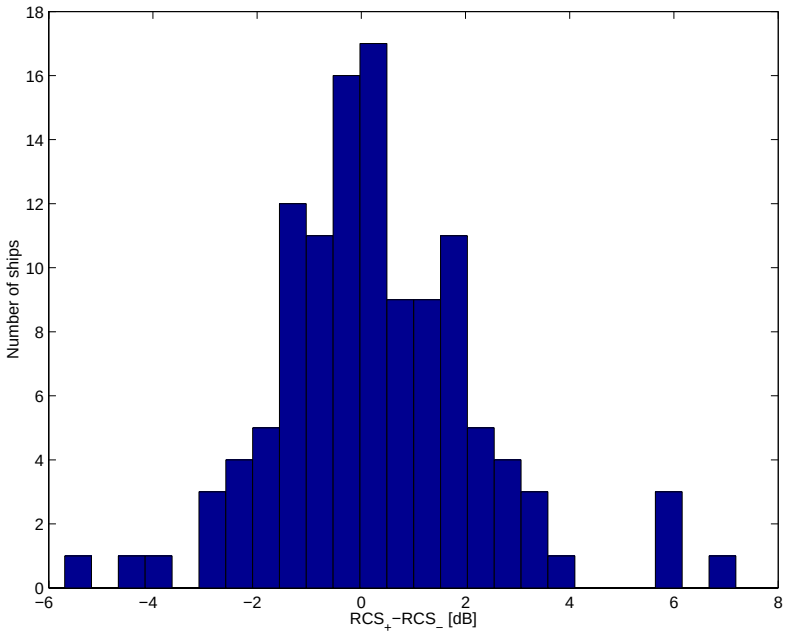

Figure 37: Histogram of differences between ship RCS estimates from two symmetrical azimuth looks.

5. Conclusions

We have considered the CHASP processing of a statistically significant number of validated ships in R-1 Fine mode data. Ship validation information was available via AISLive. We focussed on a limited number of scenes of the Strait of Dover area since they offer rather high information content (i.e., 121 validated ships in just seven separate scenes). The main objectives of the work were to examine the applicability of CHASP and to identify methods that are appropriate to R-1 and R-2 SAR processing of moving ships.

Most of the analysis was carried out using range-compressed (RC) data, rather than single look complex (SLC) data that would be available as a routine product from a commercial SAR processor. While most of the algorithms considered could work with SLC data, additional complexity is introduced since the internal details of the SAR processor must be completely known. Furthermore, SLC data has had several filtering operations applied, which could reduce the information content, especially for moving targets. In general, we recommend that adaptive ship data analysis start from RC data. Note that this product would normally exist at some point within the processor, and its use would remove most of the book keeping and auxiliary data processing requirements from the adaptive processor.

CHASP was initially developed for processing of airborne SAR data. In this work, CHASP was revised to provide geo-referencing and calibrated data for the R-1 case. Not all CHASP algorithms apply to spaceborne SAR data, but our analysis shows that significantly more ship information is available by using adaptive processing algorithms than can be deduced from image analysis alone.

The most important outcome is that frequency tracking of the ship signature relative to the background clutter can provide an accurate estimate of the ship radial speed under broad conditions. Normally, radial speed estimation relies upon the azimuth shift of the ship target relative to the ship wake location. The problem with the ship wake approach is that wakes are rather rarely visible in R-1 data. The frequency tracking method experiences problems when the background clutter level is very low; this was a rare occurrence in the data set considered. On the other hand, ship wakes were not routinely visible in any of the seven scenes considered.

The following specific conclusions arise from the analysis presented in this document:

- CHASP can provide useful ship information through a very fast, chip-based analysis;
- Radial speed can be estimated to within ±2 m/s;
- Radial speed estimation accuracy could be improved through use of better ocean clutter models;
- Radial speed results should be better for a zero-Doppler steered SAR (e.g., for R-2) since there is less need for RCMC, but clutter DC estimation should still be used to improve precision;
- Radial speed estimation accuracy cannot be guaranteed when using SLC data as input because SLC processing typically includes (perhaps unknown) reshaping of the Doppler spectrum;

- The ratio of the along-track speed to the SAR effective speed, along with the short aperture, limit the sensitivity of the Map-drift and similar algorithms; they are probably not reliable enough for R-1 or R-2 processing;
- Estimation of vessel orientation from the ship signature is possible, at least for vessels over 50 m in length in Fine beam mode data, even with the simple and fast CHASP method;
- Aspect angle estimation may be ambiguous, especially for slow moving or azimuth travelling ships;
- Azimuth travelling ships are readily recognised through several features (azimuth elongation of the ship signature in the image domain, high modulation index of the power envelope in slow time, and a low confidence measure for the aspect angle estimate);
- Azimuth travelling ships are difficult cases for length and speed estimation;
- RCS is generally well estimated for both range and azimuth travelling vessels (the aspect angle may play a minor role);
- The impact of elevation angle on ship RCS cannot be assessed from this data set (there is a rather small range of incidence angles for R-1 Fine mode);
- When RCS is estimated from multi-look images, the applied normalization strategy may influence the result to a small extent; this should be a minor concern for standard (i.e., calibrated) products, but should be reviewed and tested for multi-looking from SLC images; and
- Processing experiments have not revealed any systematic changes in ship RCS with resolution.

While the analysis in this document has focussed on R-1 Fine mode data, it should be noted that the CHASP algorithms should apply equally well to lower resolution modes, as will be adopted for operational maritime surveillance using R-2. It is recommended that CHASP-like algorithms be considered for operational use in this context, with RC data as the starting point for CHASP-like processing. Additional tests with lower resolution data are warranted.

Annex A σ° Maps

This Annex contains maps that are proportional to σ° for each of the Dover scenes considered.

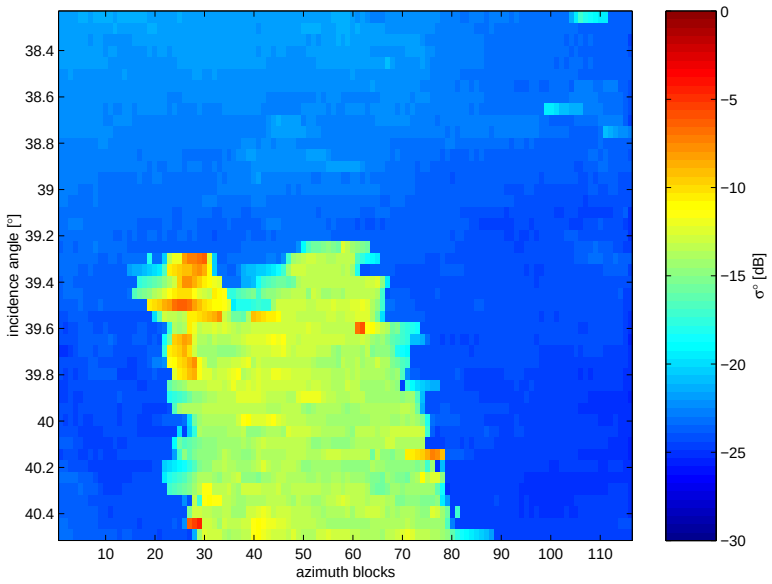

Figure 38: σ° map for Scene 1.

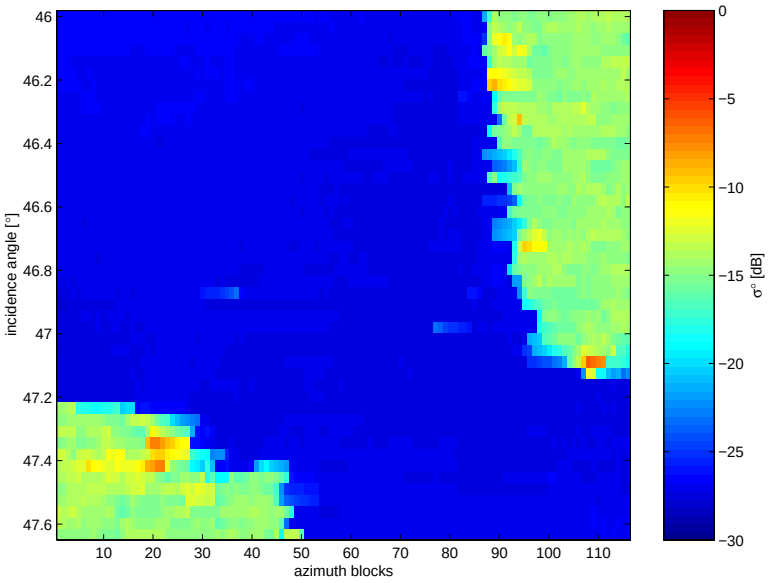

Figure 39: σ° map for Scene 2.

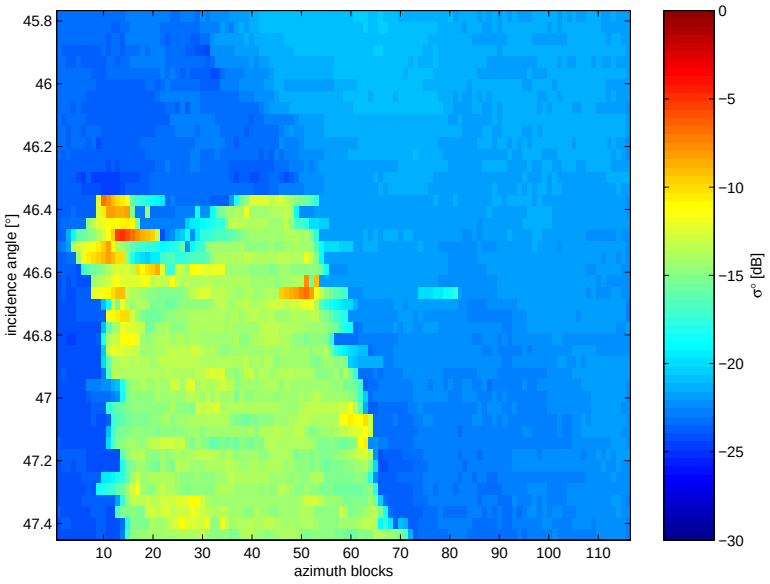

Figure 40: σ° map for Scene 3.

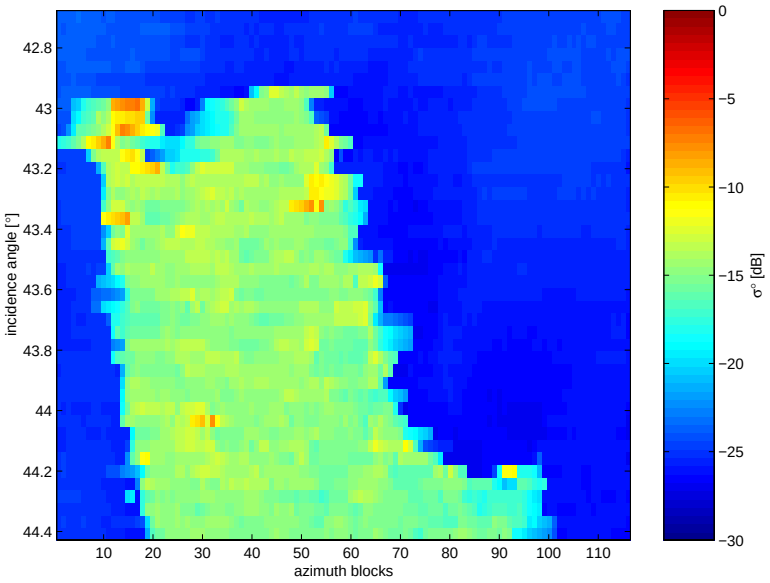

Figure 41: σ° map for Scene 4.

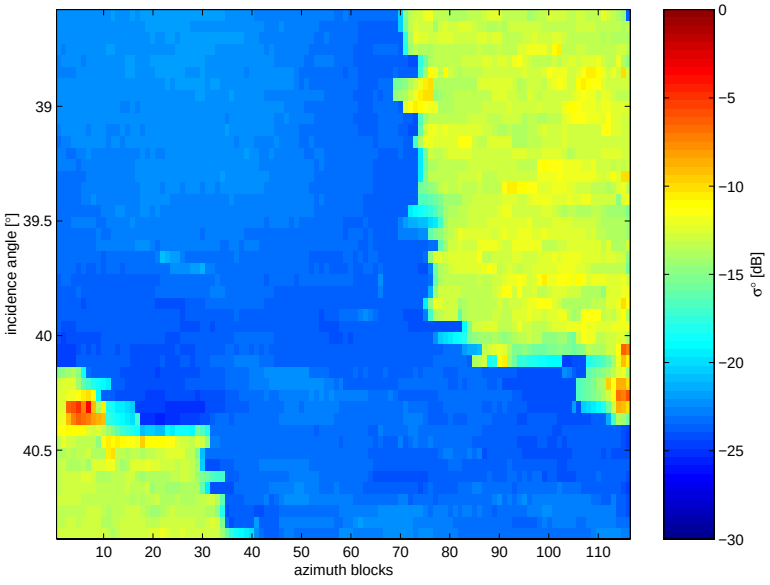

Figure 42: σ° map for Scene 5.

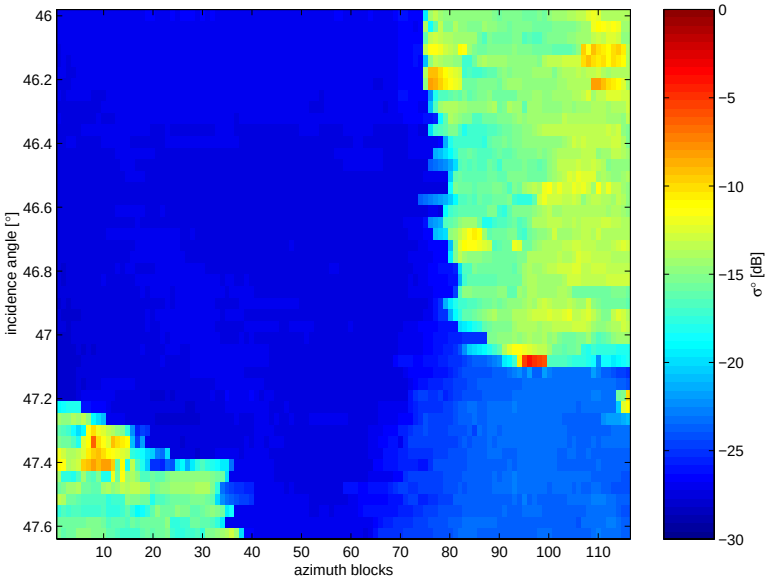

Figure 43: σ° map for Scene 6.

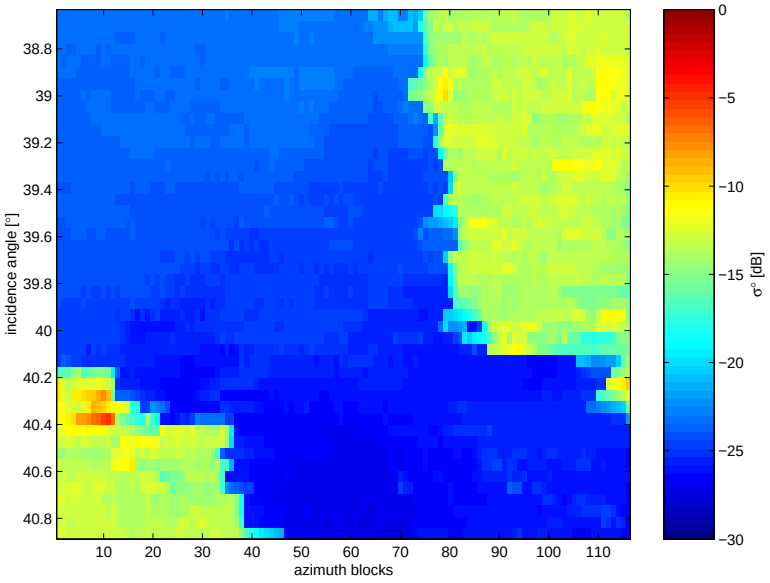

Figure 44: σ° map for Scene 7.

Annex B CDC Maps

This Annex contains CDC maps for each of the Dover scenes considered.

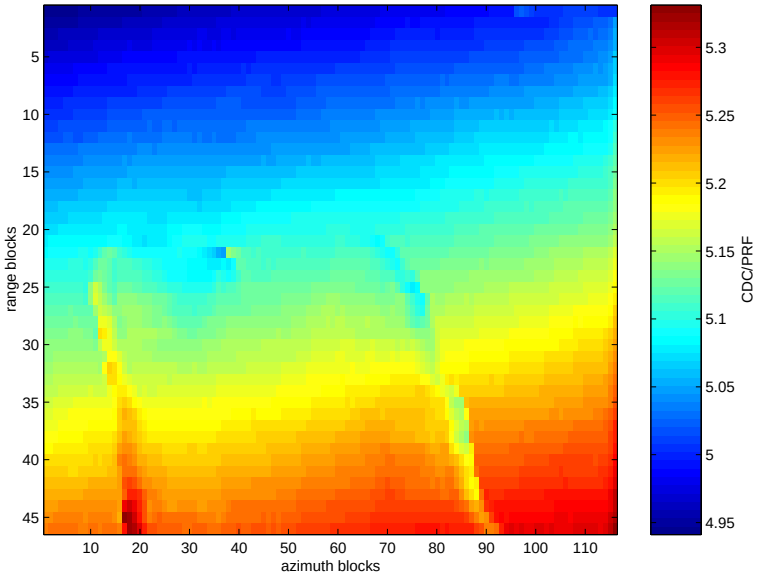

Figure 45: CDC map for Scene 1.

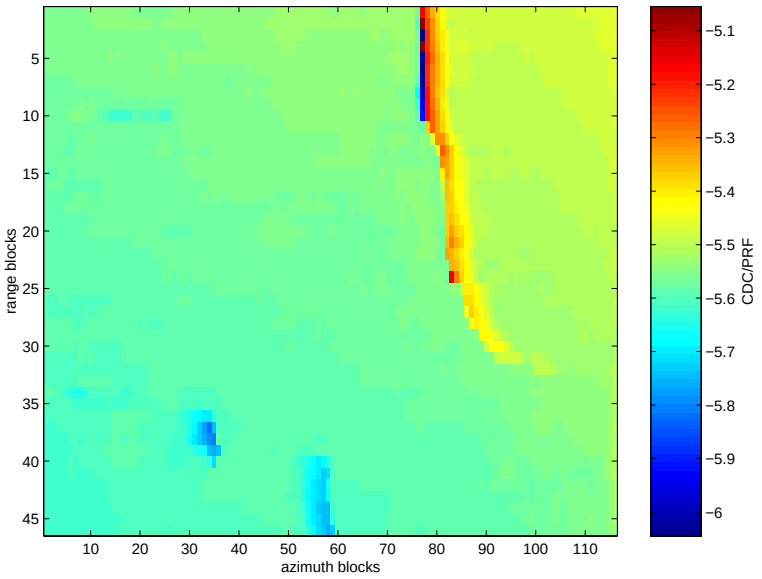

Figure 46: CDC map for Scene 2.

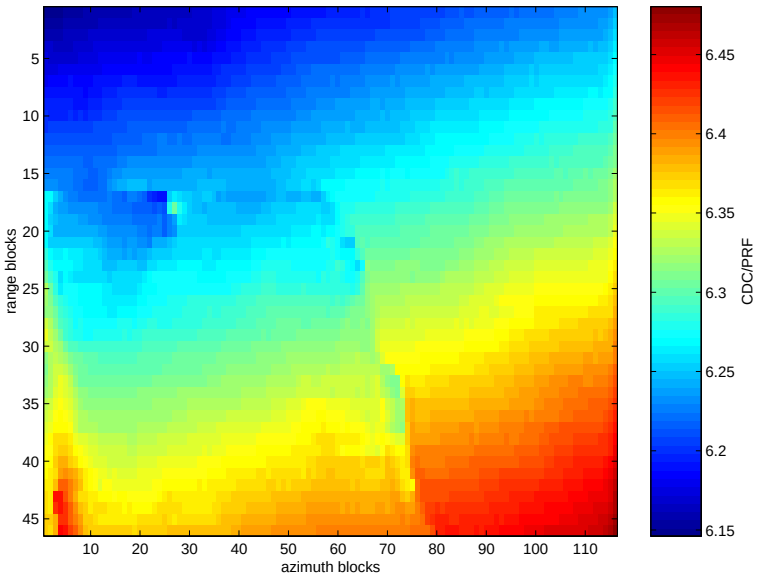

Figure 47: CDC map for Scene 3.

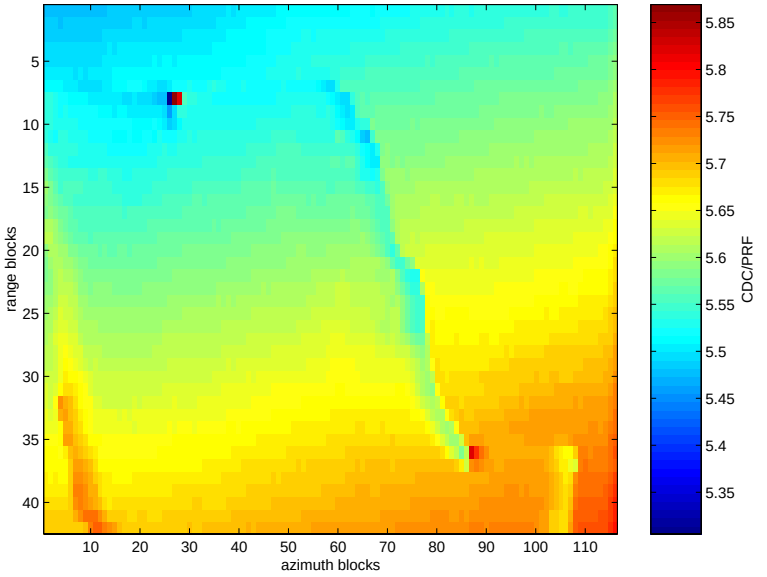

Figure 48: CDC map for Scene 4.

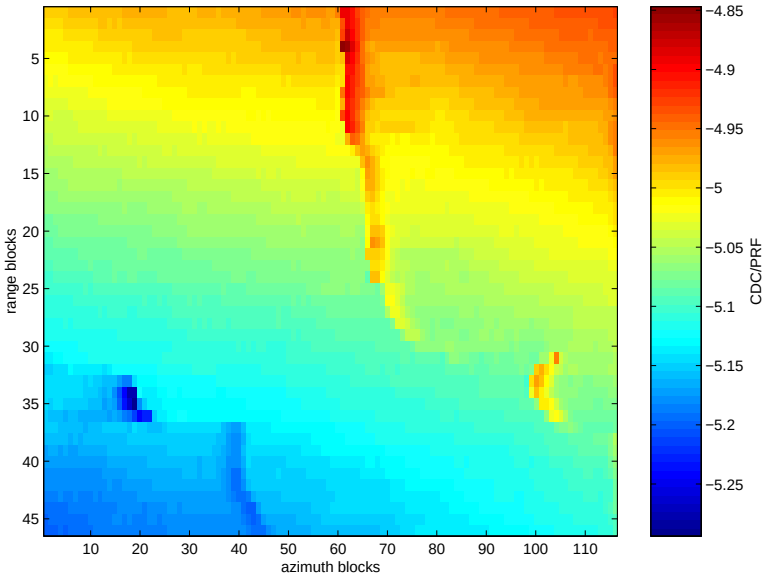

Figure 49: CDC map for Scene 5.

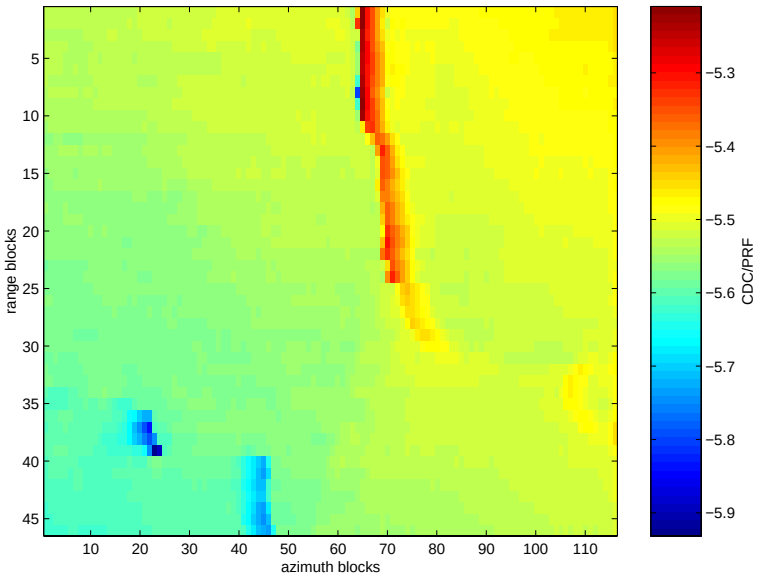

Figure 50: CDC map for Scene 6.

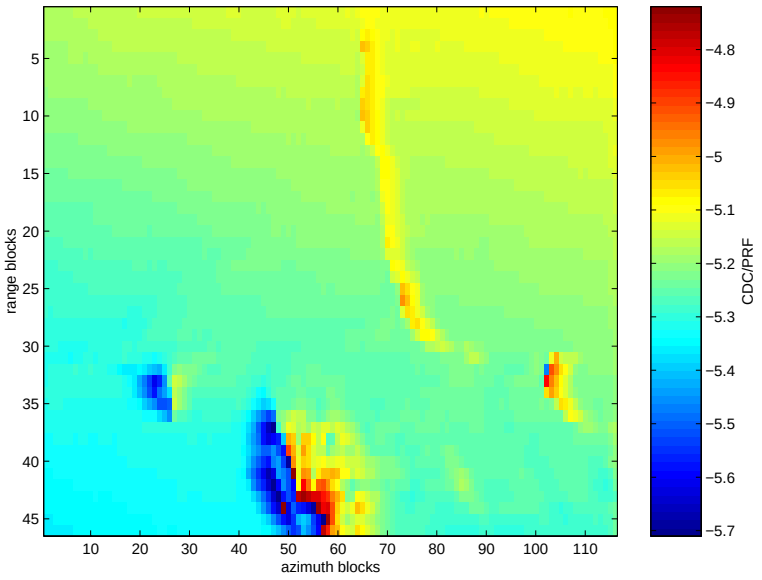

Figure 51: CDC map for Scene 7.

Annex C CDC Transects

This Annex contains representative CDC transects across each of the Dover scenes considered.

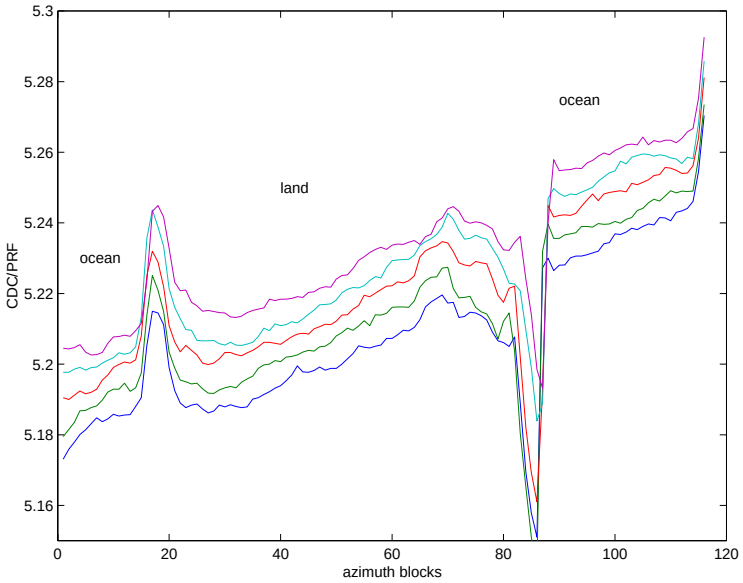

Figure 52: Along-track variation of CDC for several adjacent range bins for Scene 1.

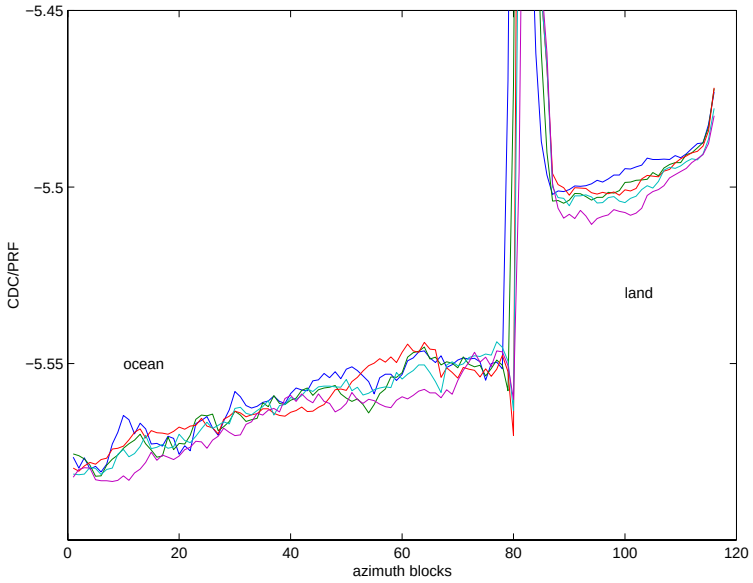

Figure 53: Along-track variation of CDC for several adjacent range bins for Scene 2.

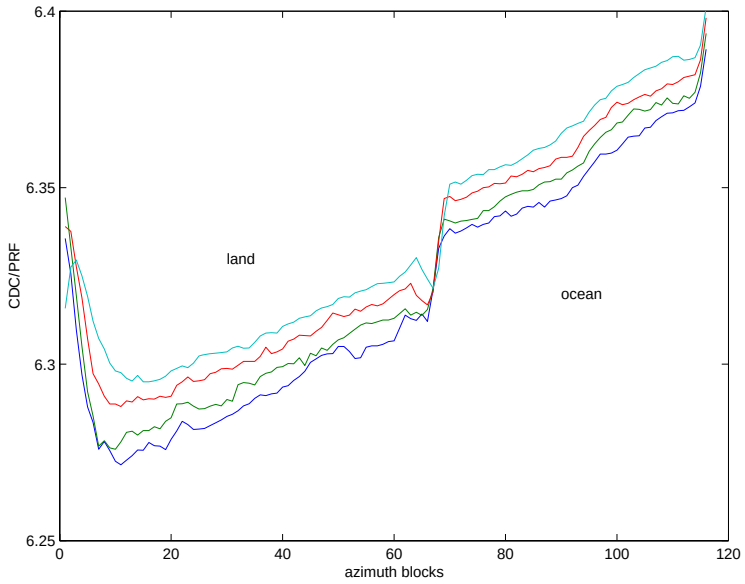

Figure 54: Along-track variation of CDC for several adjacent range bins for Scene 3.

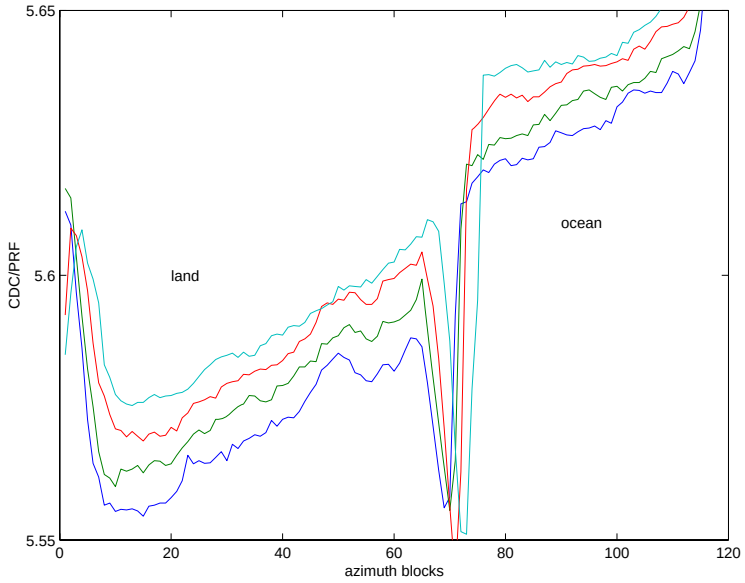

Figure 55: Along-track variation of CDC for several adjacent range bins for Scene 4.

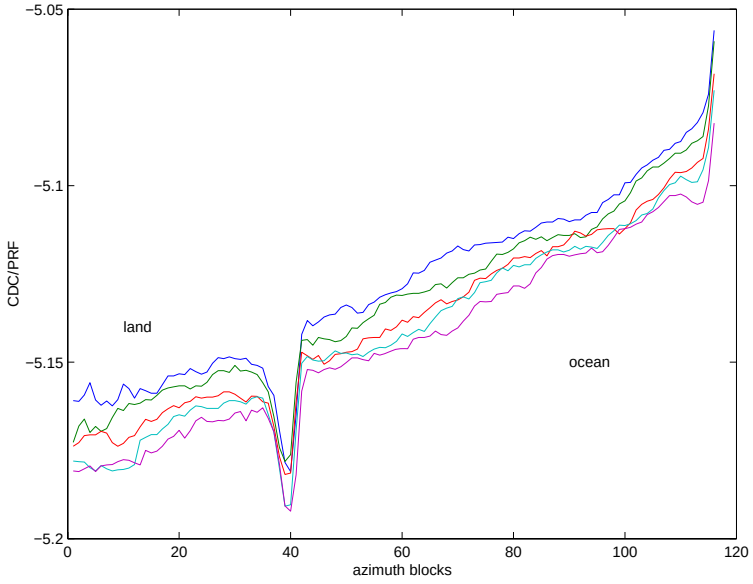

Figure 56: Along-track variation of CDC for several adjacent range bins for Scene 5.

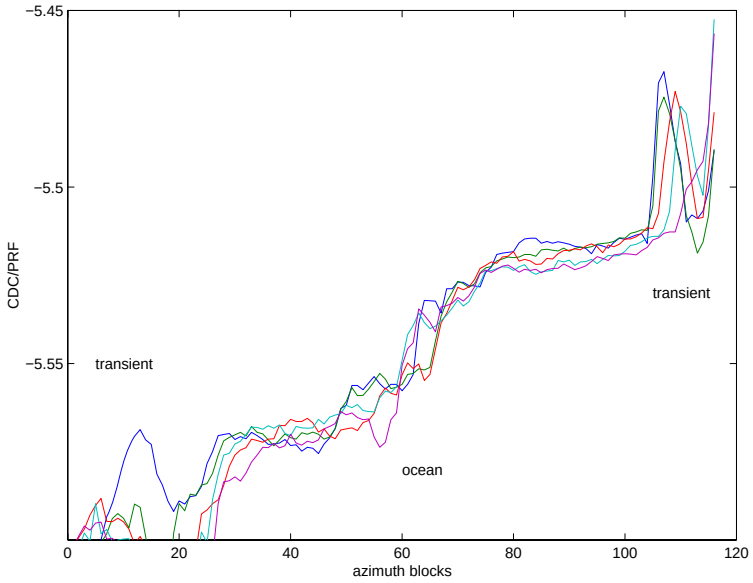

Figure 57: Along-track variation of CDC for several adjacent range bins for Scene 6.

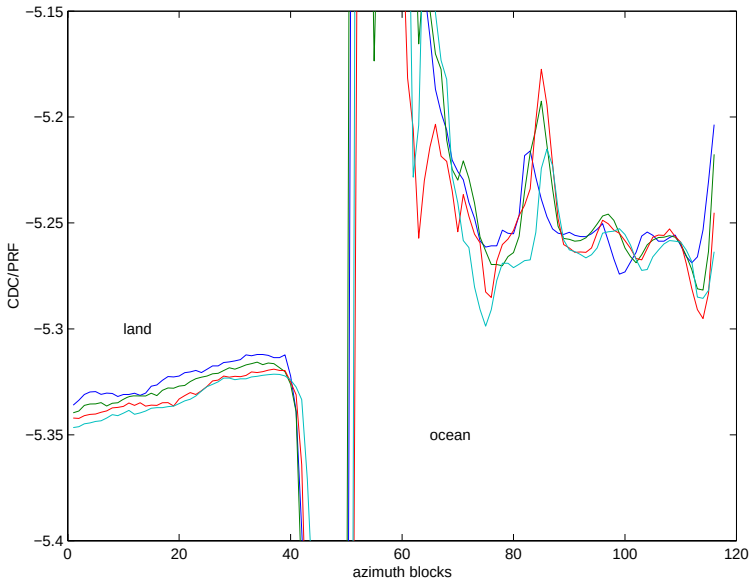

Figure 58: Along-track variation of CDC for several adjacent range bins for Scene 7.

Annex D Examples of Processed Ships

This Annex contains some examples of the processed ships in the various Dover scenes considered. The ship designation is D<d>S<s> where d is the Dover Scene number and s is the arbitrary ship number within the particular Scene. In each case, azimuth is from top-to-bottom and increasing range is from left-to-right.

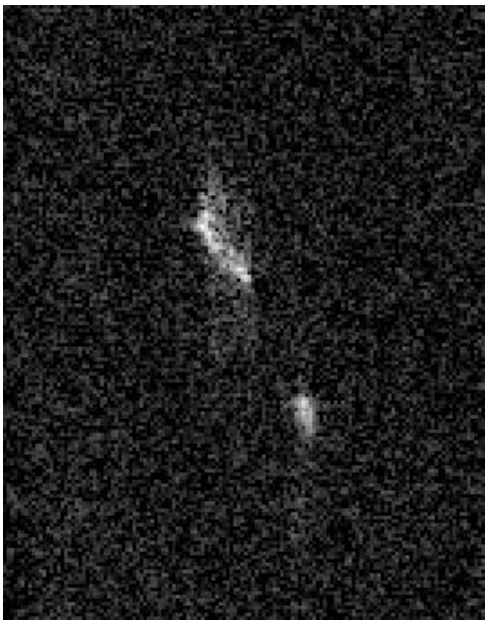

Figure 59: D5S19, the 34 m long tug boat "AHT Braveheart", seen here towing a large barge, is the smallest ship in the data set.

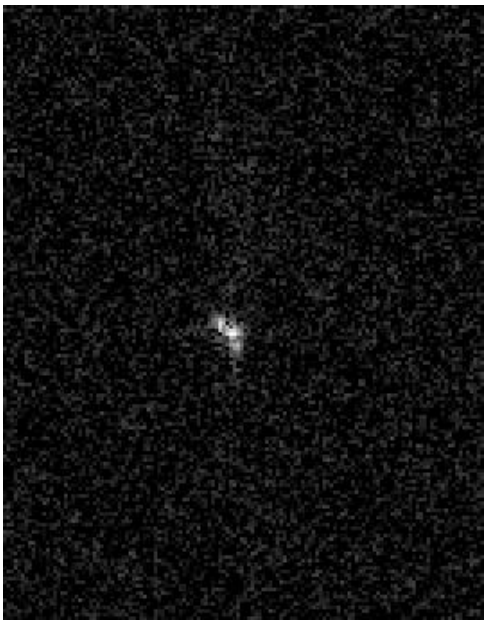

Figure 60: D7S1, the 63 m long freighter "Germa" is one of the smallest ships in the data set.

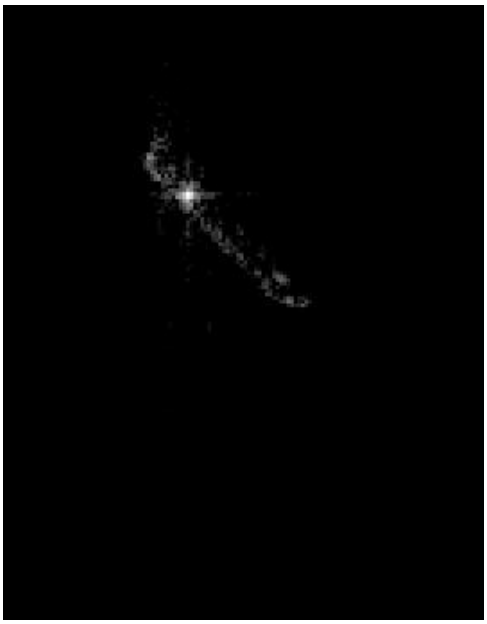

Figure 61: D6S1, the 347 m long cargo ship "Chastine Maersk" is one of the largest ships in the data set.

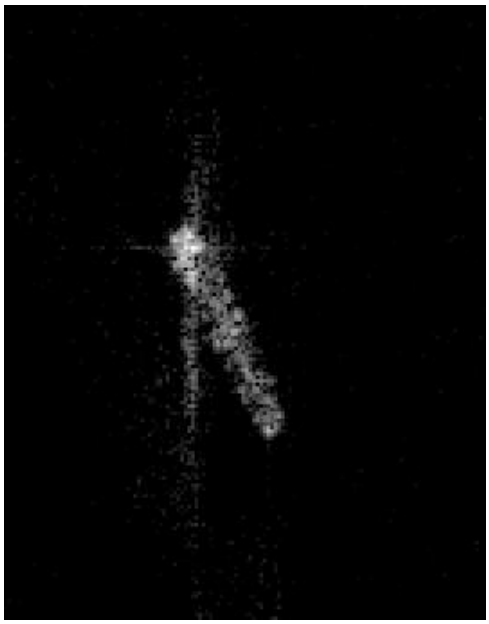

Figure 62: D4S19, the 332 m long tanker "Neptune Glory" is one of the largest ships in the data set.

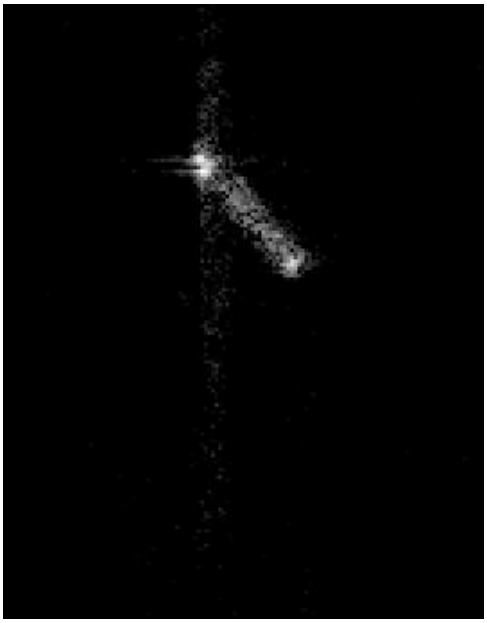

Figure 63: D6S27, a ship with a poor V_r estimate but a good DC estimate.

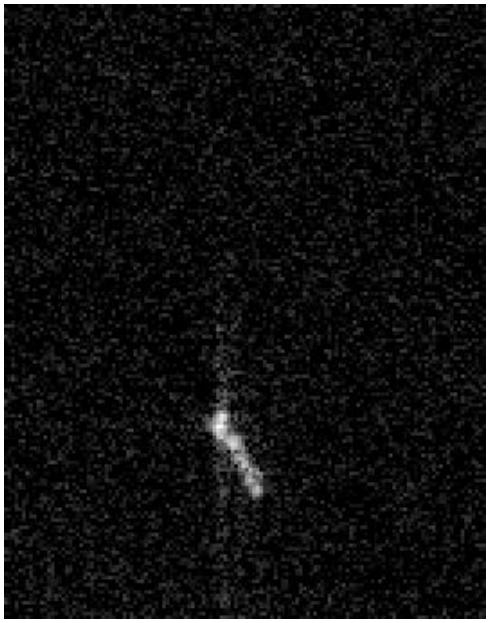

Figure 64: D7S34, a ship with a poor V_r estimate but a good DC estimate.

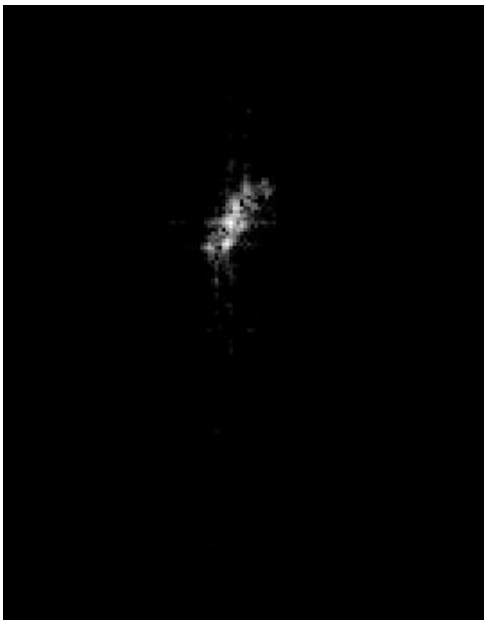

Figure 65: D7S8, a ship with a poor V_r estimate.

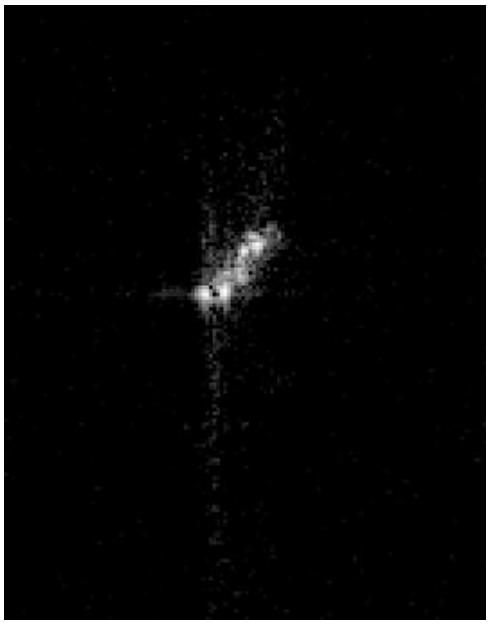

Figure 66: D6S5, the same ship as D7S8, but with a good V_r estimate.

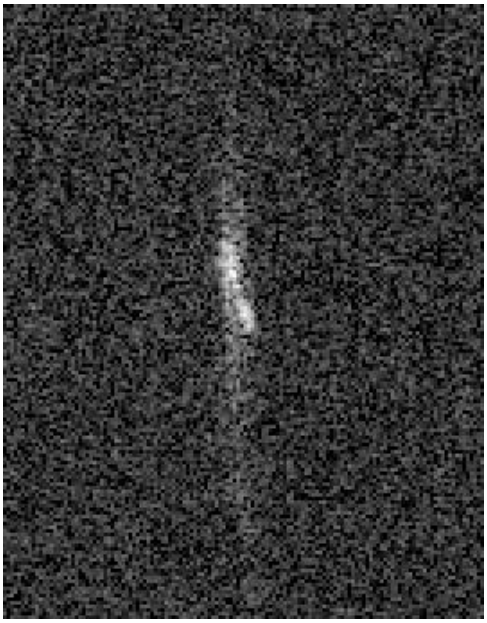

Figure 67: D2S2, a slow moving ship with a 180° direction error.

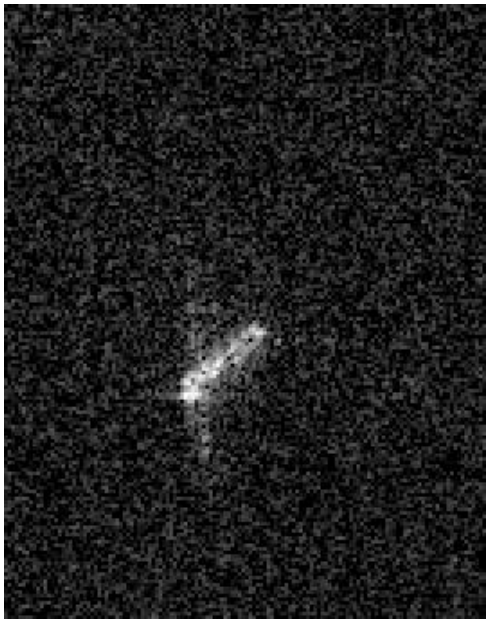

Figure 68: D5S4, a slow moving ship with a 180° direction error.

Figure 69: D3S15, a ship with an incorrect aspect angle for no apparent reason.

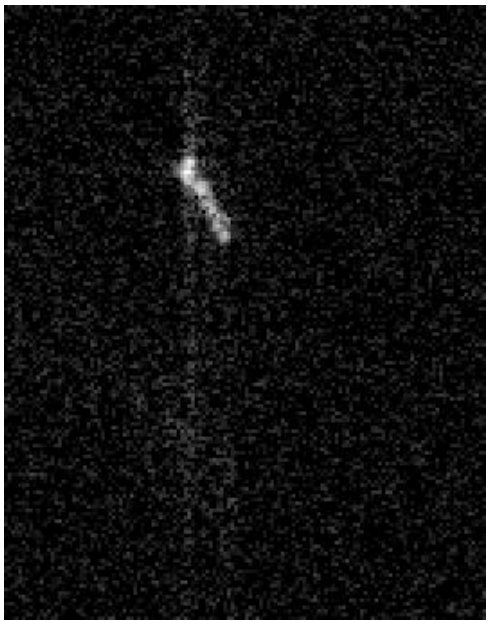

Figure 70: D7S34, a ship with an incorrect aspect angle for no apparent reason.

Annex E Georeferencing Comparisons

This Annex contains plots of SAR-estimated ship locations and AIS-derived ship locations for each of the Dover scenes considered. The plots permit a visual evaluation of the CHASP georeferencing algorithm.

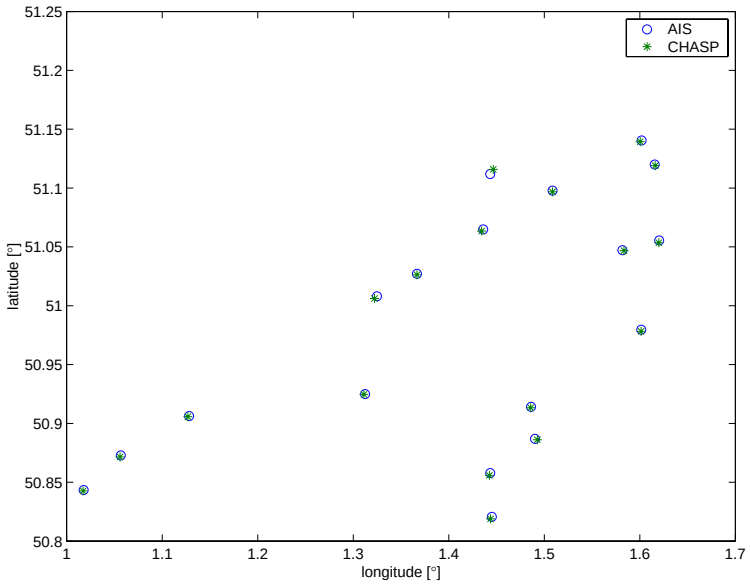

Figure 71: Geolocation of ships predicted from AIS data and reported by CHASP for Scene 1.

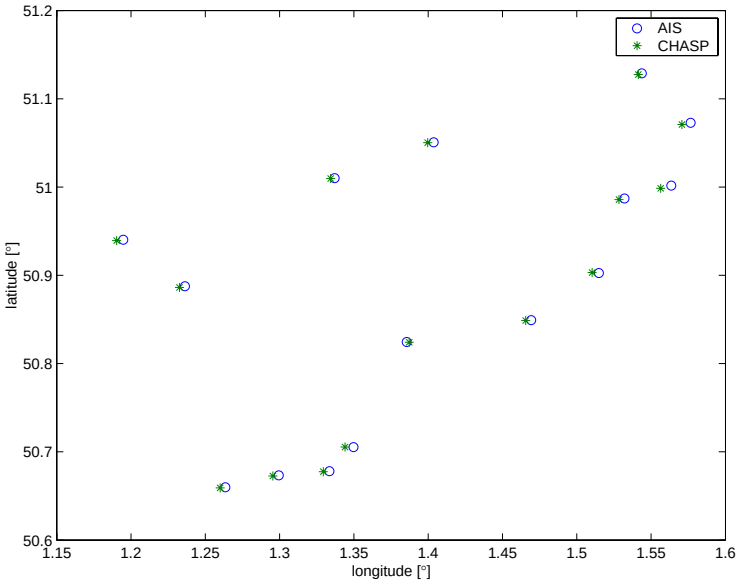

Figure 72: Geolocation of ships predicted from AIS data and reported by CHASP for Scene 2.

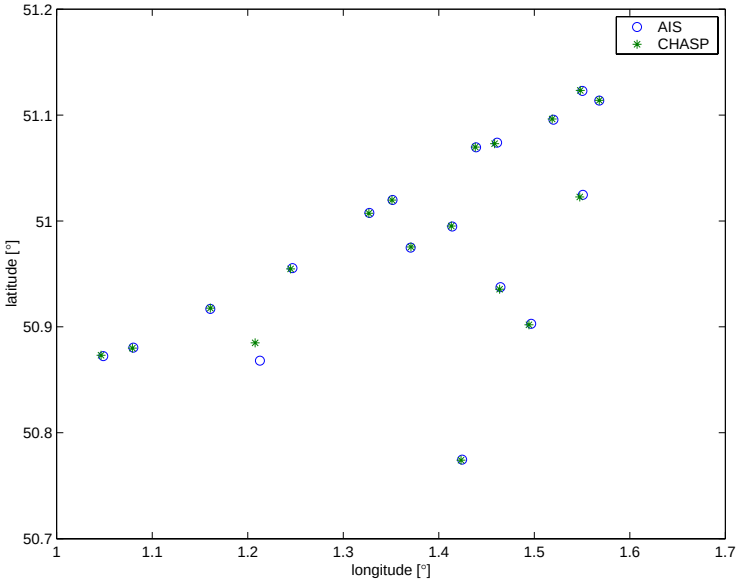

Figure 73: Geolocation of ships predicted from AIS data and reported by CHASP for Scene 3.

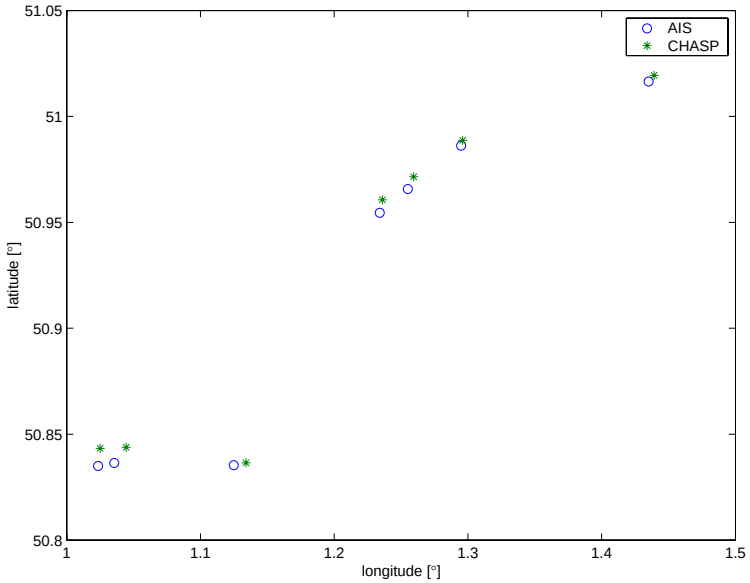

Figure 74: Geolocation of ships predicted from AIS data and reported by CHASP for Scene 4.

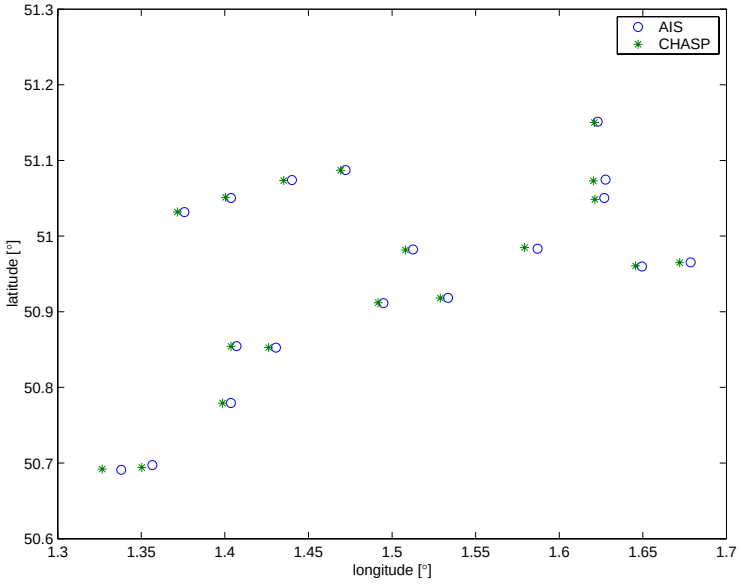

Figure 75: Geolocation of ships predicted from AIS data and reported by CHASP for Scene 5.

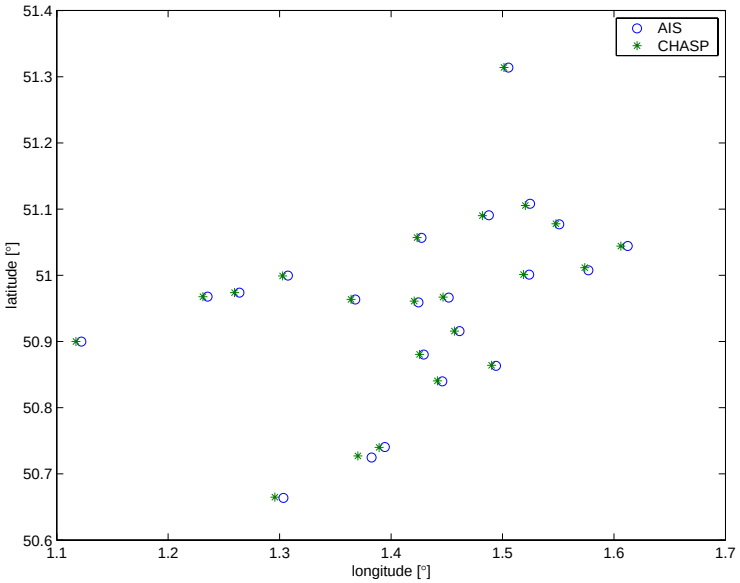

Figure 76: Geolocation of ships predicted from AIS data and reported by CHASP for Scene 6.

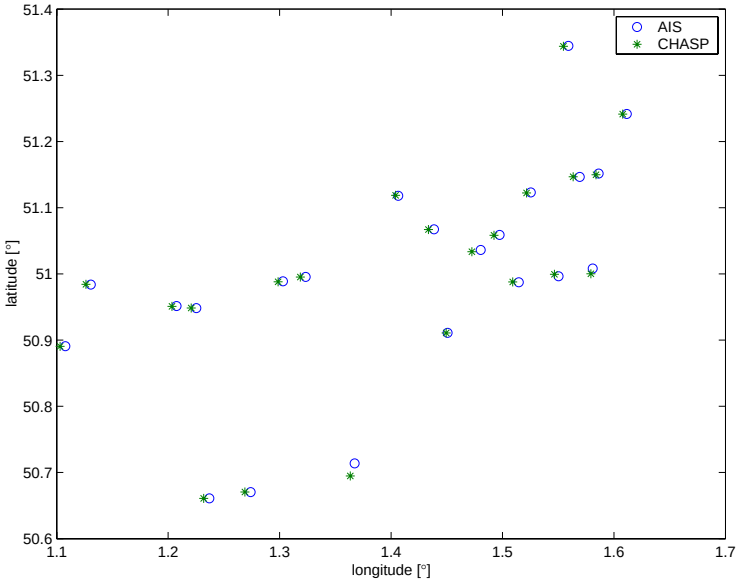

Figure 77: Geolocation of ships predicted from AIS data and reported by CHASP for Scene 7.

Annex F Radial Speed Error Histograms

This Annex contains histogram plots of the radial speed error for each of the Dover scenes considered.

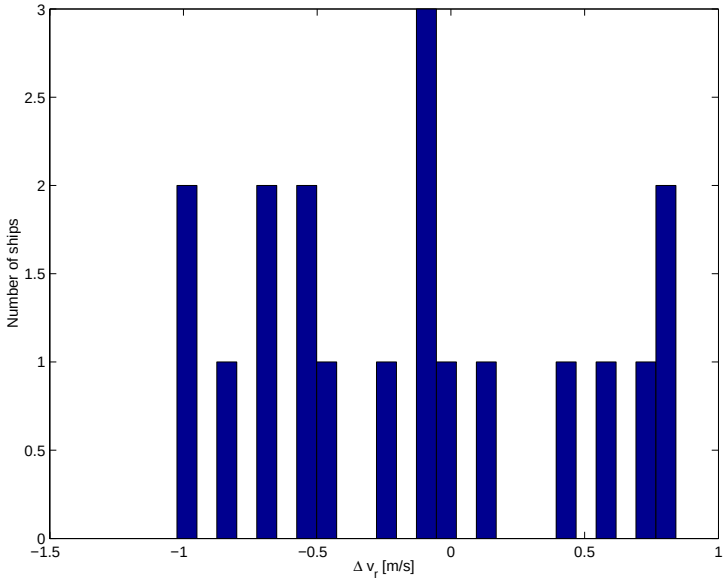

Figure 78: Histogram of radial speed errors for Scene 1.

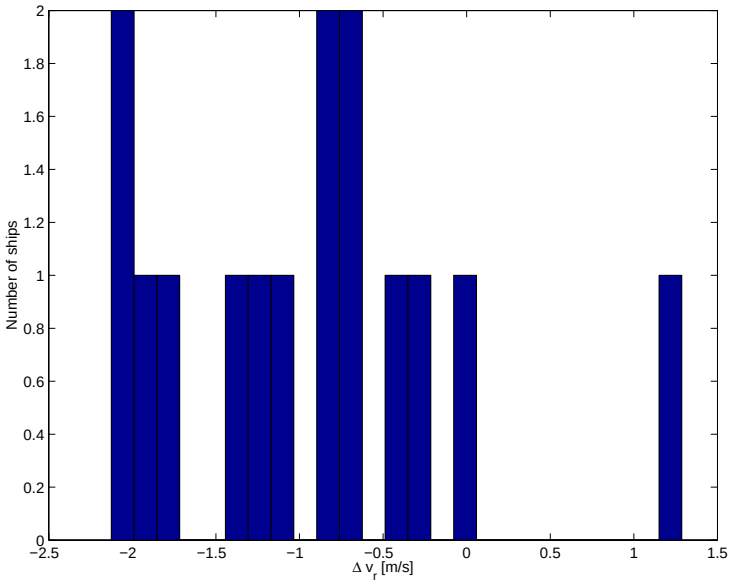

Figure 79: Histogram of radial speed errors for Scene 2.

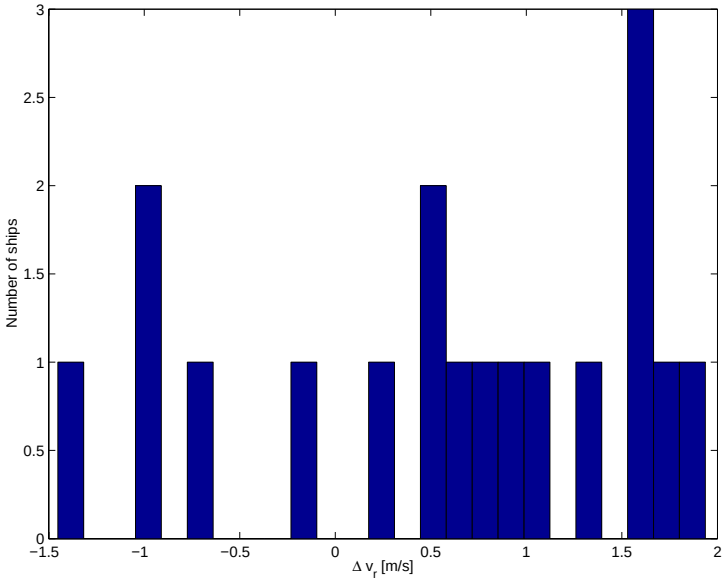

Figure 80: Histogram of radial speed errors for Scene 3.

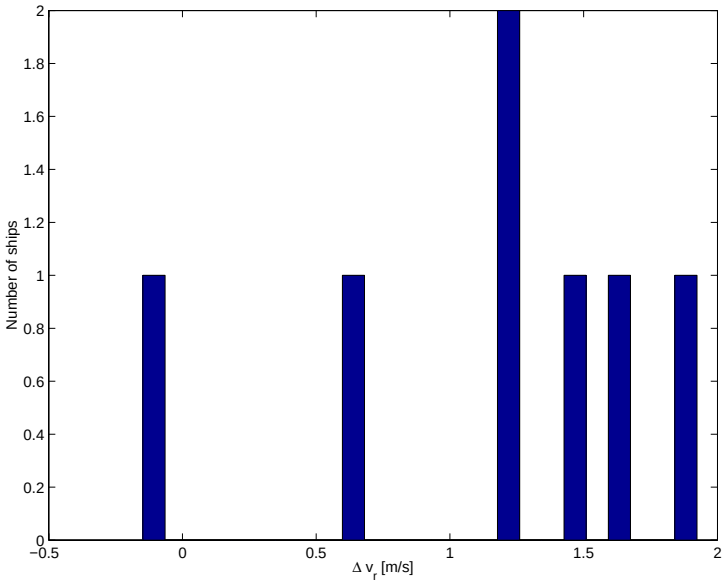

Figure 81: Histogram of radial speed errors for Scene 4.

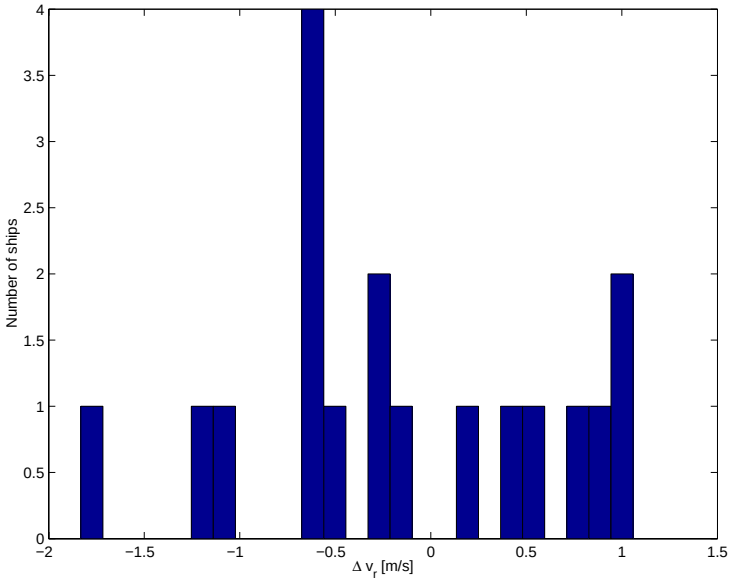

Figure 82: Histogram of radial speed errors for Scene 5.

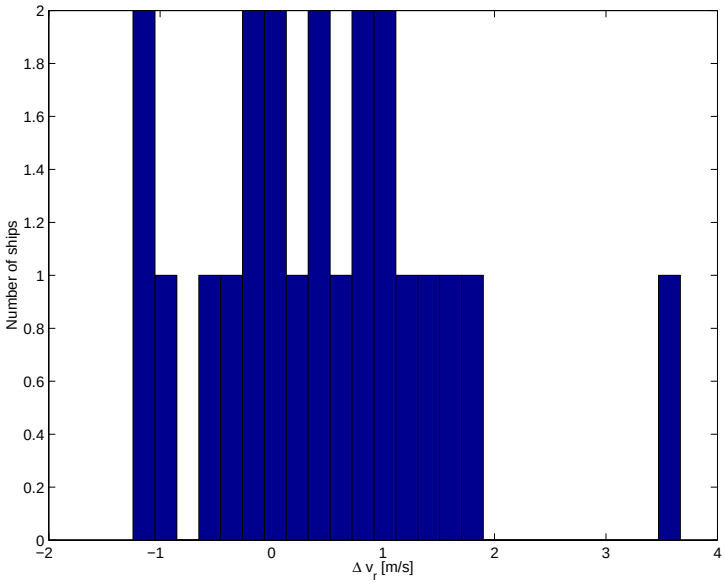

Figure 83: Histogram of radial speed errors for Scene 6.

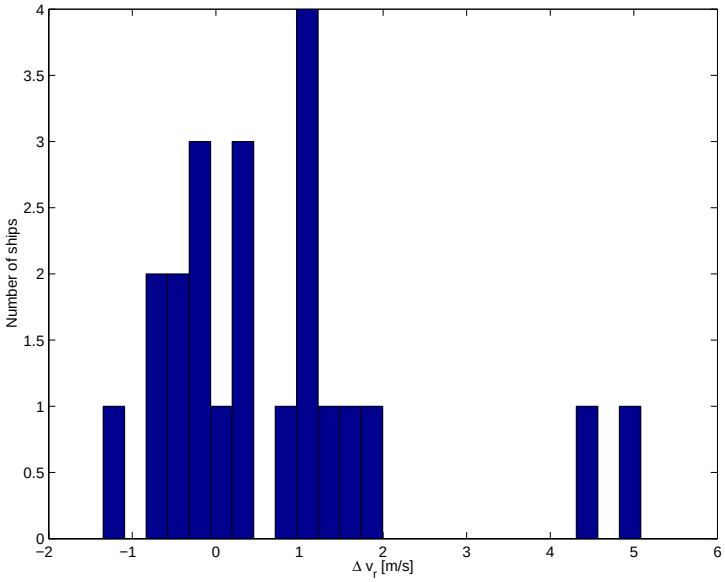

Figure 84: Histogram of radial speed errors for Scene 7.

Annex G Radial Speed Error and Location

This Annex contains plots that show the ship locations and the associated radial speed estimation error for each of the Dover scenes considered. A coarse land mask has been employed.

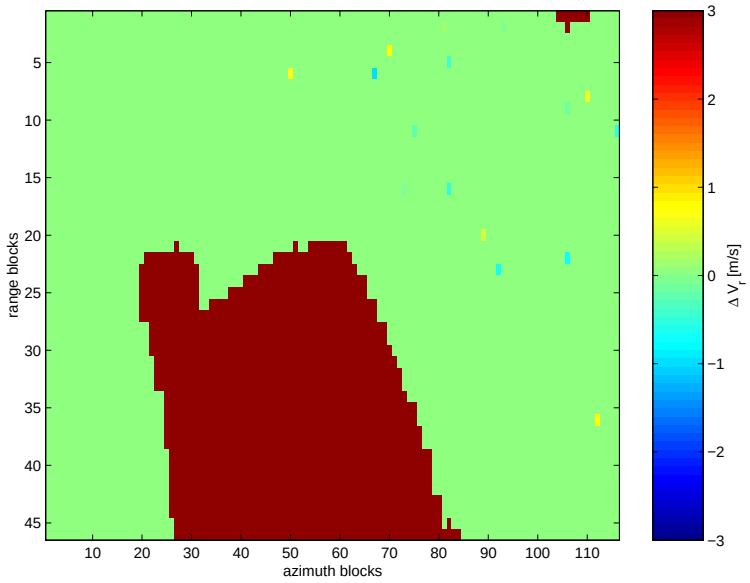

Figure 85: Radial speed estimation error for Scene 1.

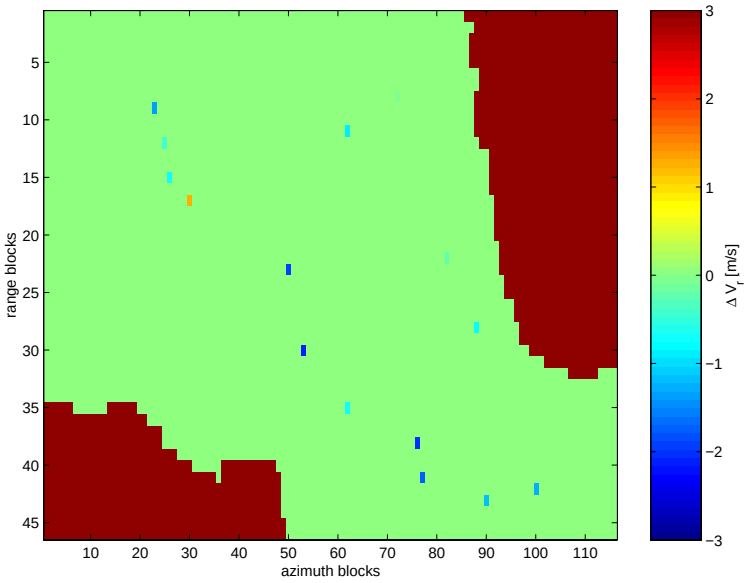

Figure 86: Radial speed estimation error for Scene 2..

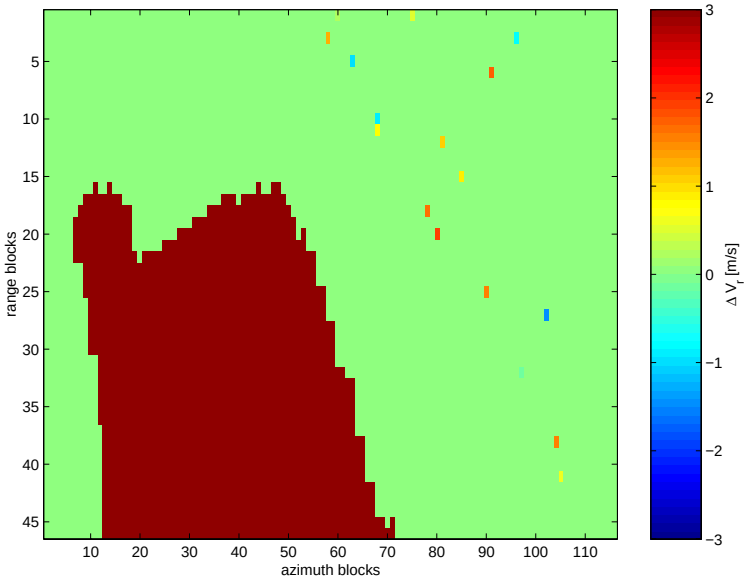

Figure 87: Radial speed estimation error for Scene 3.

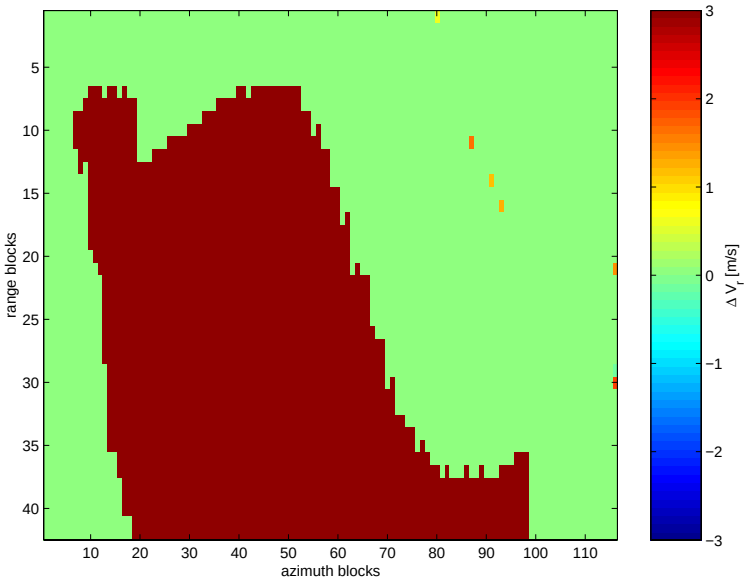

Figure 88: Radial speed estimation error for Scene 4.

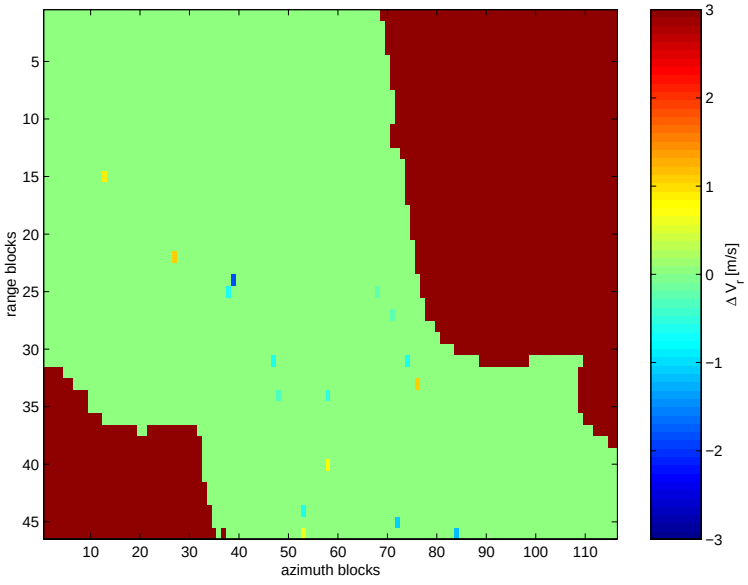

Figure 89: Radial speed estimation error for Scene 5.

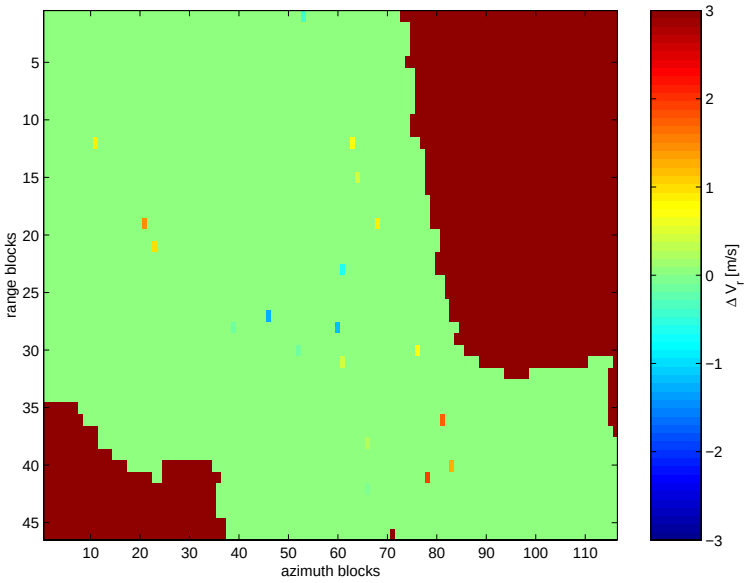

Figure 90: Radial speed estimation error for Scene 6.

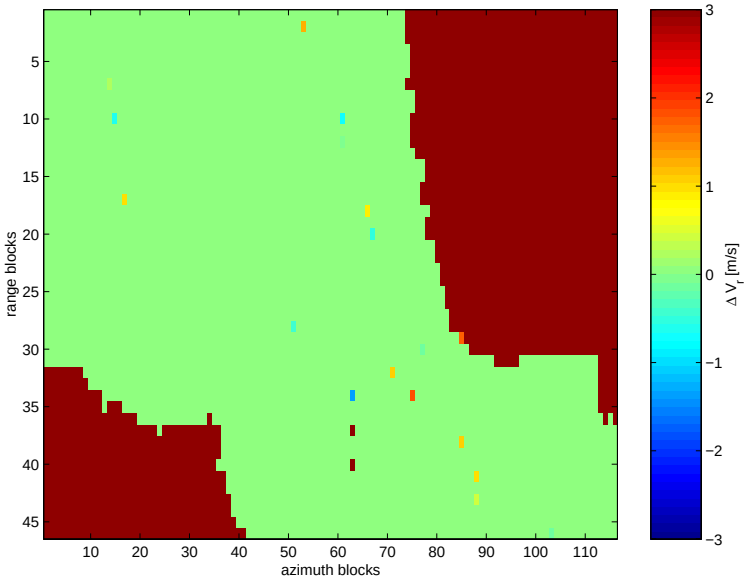

Figure 91: Radial speed estimation error for Scene 7.

Annex H Examples of Ships at Various Aspect Angles

This Annex contains examples of four ships that were imaged at various aspect angles that illustrate the performance of the region-growing algorithm for ship aspect angle estimation.

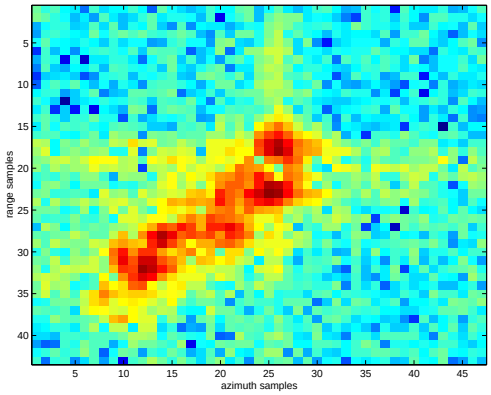

Figure 92: Image window with a ship at an aspect angle of 38°.

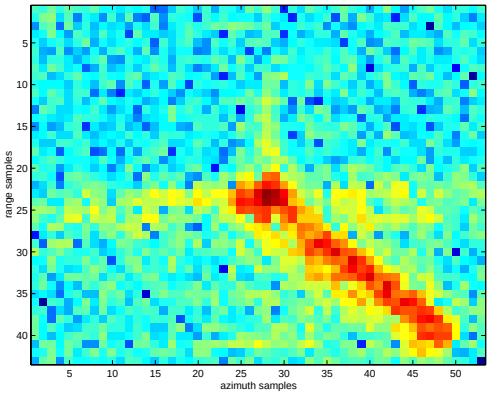

Figure 93: Image window with a ship at an aspect angle of 315°.

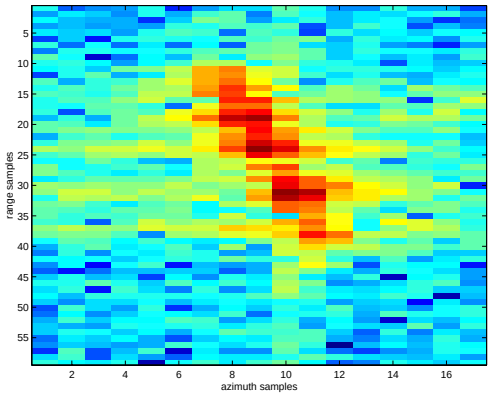

Figure 94: Image window with a ship at an aspect angle of 171°.

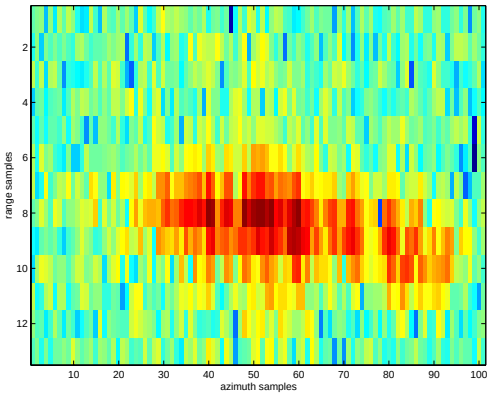

Figure 95: Image window with a ship at an aspect angle of 268°.

Annex I Examples of Ship Focus

This Annex contains examples of three ships that illustrate the impact of focus improvement through adaptive processing. Although the change in the ship contrast permits estimation of the ship velocity, as shown in Table 3, the visual impact, as shown in Figure 96 through Figure 98, is minimal.

Table 3: Ship parameters for focus examples.

Ship	L [m]	AIS V_r [m/s]	CHASP V_r [m/s]	AIS V_a [m/s]	CHASP V_a [m/s]
D1S7	180	6.4	6.4	2.8	3.8
D1S32	127	–2.1	–2.1	4.7	4.1
D7S6	130	2.5	3.5	8.6	8.6

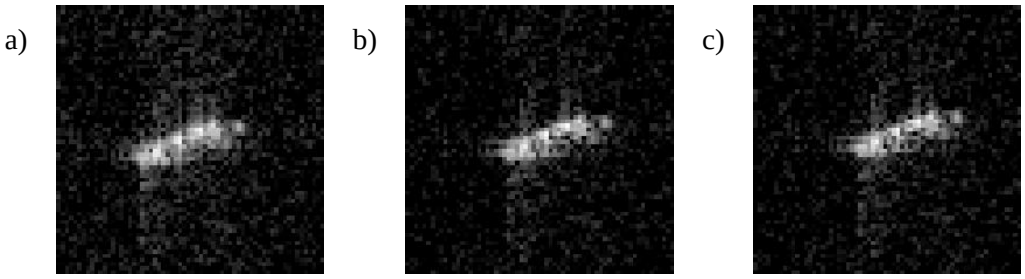

Figure 96: Ship D1S7: a) nominal parameters; b) adjusted DC and nominal DR; and c) adjusted parameters.

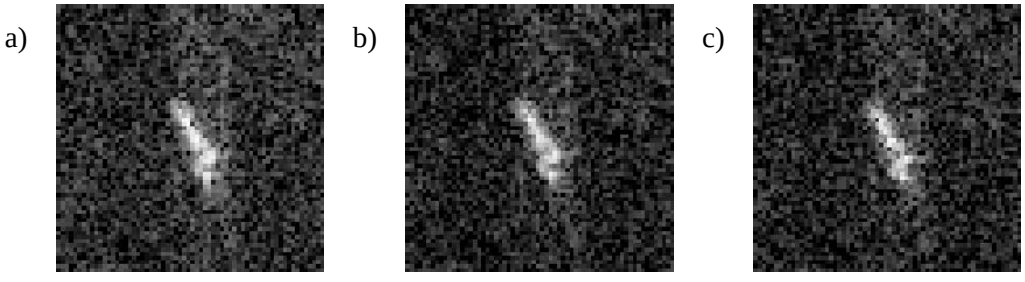

Figure 97: Ship D1S32: a) nominal parameters; b) adjusted DC and nominal DR; and c) adjusted parameters.

a) b) c)

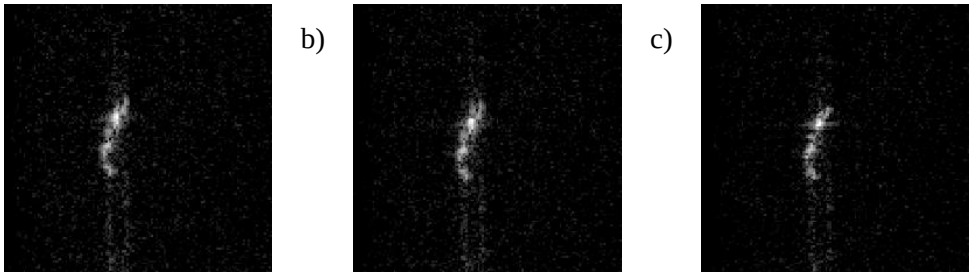

Figure 98: Ship D7S6: a) nominal parameters; b) adjusted DC and nominal DR; and c) adjusted parameters.

References

[1] Vachon, P.W., J.W.M. Campbell, C. Bjerkelund, F.W. Dobson, and M.T. Rey, "Ship detection by the RADARSAT SAR: Validation of detection model predictions", *Canadian Journal of Remote Sensing*, Vol. 23, No. 1, pp. 48-59, 1997.

[2] Vachon, P.W., and M. Dragošević (2006), COASP and CHASP Processors for Strip-map and Moving Target Adaptive Processing of EC CV-580 Synthetic Aperture Radar Data: Algorithms and Software Description, (DRDC Ottawa TM 2006-066) Defence R&D Canada – Ottawa.

[3] Vachon, P.W., M. Dragošević, N. Kashyap, C. Liu, D. Schlingmeier, A. Meek, T. Potter, B. Yue, and J. Kraft (2006), Processing and Analysis of Polarimetric Ship Signatures from MARSIE: Report on Results for Polar Epsilon, (DRDC Ottawa TM 2006-202) Defence R&D Canada – Ottawa.

[4] Vachon, P.W., R.A. English, and J. Wolfe, "Validation of RADARSAT-1 Vessel Signatures with AISLive Data", in press, *Canadian Journal of Remote Sensing*, 2007.

List of acronyms

AIS	Automatic Identification System
CDC	Clutter Doppler Centroid
CHASP	Chip-based Adaptive SAR Processor
CSA	Canadian Space Agency
CV-580	Convair 580 (aircraft)
D#	Dover scene # (1 through 7), e.g., D1 refers to Dover scene 1
DC	Doppler Centroid
DND	Department of National Defence
DR	Doppler Rate
EC	Environment Canada
F#	R-1 Fine mode # (1 through 5)
FS	Sampling Frequency
L	Ship length
M	Aspect angle and confidence indicator
NSR	Near edge Slant Range
PRF	Pulse Repetition Frequency
PTR	Point Target Response
R-1	RADARSAT-1
R-2	RADARSAT-2
R&D	Research & Development
RC	Range Compressed (i.e., azimuth non-compressed)
RCMC	Range Cell Migration Correction
RCS	Radar Cross Section
S#	Arbitrary ship # within a particular Dover scene, e.g., D1S7 refers to ship #7 in Dover scene #1
SAR	Synthetic Aperture Radar
SLC	Single Look Complex
SV	State Vector
V_a	Target azimuthal velocity component
V_r	Target radial velocity component

This page intentionally left blank.

Distribution list

Document No.: DRDC Ottawa TM 2007-053

LIST PART 1: Internal Distribution by Centre:

4 Library DRDC Ottawa
1 Marina Dragošević
1 Gary Geling
1 Chuck Livingstone
1 Jeff Secker
1 Paris Vachon

8 TOTAL LIST PART 1

LIST PART 2: External Distribution by DRDKIM

1 CISTI
1 DRDKIM
3 Library and Archives Canada
1 LCol Jeff Howes, DPDOIS, Polar Epsilon
1 LCdr Robert Quinn, DJCP
1 LCdr Andy Samoluk, DJCP
1 Jake Tunaley, DPDOIS, Polar Epsilon
1 Caroline Wilcox, DSTC4ISR

10 TOTAL LIST PART 2

18 TOTAL COPIES REQUIRED

This page intentionally left blank.

DOCUMENT CONTROL DATA

(Security classification of title, body of abstract and indexing annotation must be entered when the overall document is classified)

1. ORIGINATOR (The name and address of the organization preparing the document. Organizations for whom the document was prepared, e.g. Centre sponsoring a contractor's report, or tasking agency, are entered in section 8.)

Defence R&D Canada - Ottawa
3701 Carling Avenue
Ottawa, Ontario K1A 0Z4

2. SECURITY CLASSIFICATION (Overall security classification of the document including special warning terms if applicable.)

UNCLASSIFIED

3. TITLE (The complete document title as indicated on the title page. Its classification should be indicated by the appropriate abbreviation (S, C, R or U) in parentheses after the title.)

Adaptive Processing of RADARSAT-1 Fine Mode Data: Ship Parameter Estimation

4. AUTHORS (last name, followed by initials – ranks, titles, etc. not to be used)

Vachon, P.W., Dragošević, M.

5. DATE OF PUBLICATION (Month and year of publication of document.)

March 2007

6a. NO. OF PAGES (Total containing information, including Annexes, Appendices, etc.)

92

6b. NO. OF REFS (Total cited in document.)

4

7. DESCRIPTIVE NOTES (The category of the document, e.g. technical report, technical note or memorandum. If appropriate, enter the type of report, e.g. interim, progress, summary, annual or final. Give the inclusive dates when a specific reporting period is covered.)

Technical Memorandum

8. SPONSORING ACTIVITY (The name of the department project office or laboratory sponsoring the research and development – include address.)

Polar Epsilon Service Level Agreement

9a. PROJECT OR GRANT NO. (If appropriate, the applicable research and development project or grant number under which the document was written. Please specify whether project or grant.)

15ec06-01

9b. CONTRACT NO. (If appropriate, the applicable number under which the document was written.)

10a. ORIGINATOR'S DOCUMENT NUMBER (The official document number by which the document is identified by the originating activity. This number must be unique to this document.)

DRDC Ottawa TM 2007-053

10b. OTHER DOCUMENT NO(s). (Any other numbers which may be assigned this document either by the originator or by the sponsor.)

11. DOCUMENT AVAILABILITY (Any limitations on further dissemination of the document, other than those imposed by security classification.)

(X) Unlimited distribution
( ) Defence departments and defence contractors; further distribution only as approved
( ) Defence departments and Canadian defence contractors; further distribution only as approved
( ) Government departments and agencies; further distribution only as approved
( ) Defence departments; further distribution only as approved
( ) Other (please specify):

12. DOCUMENT ANNOUNCEMENT (Any limitation to the bibliographic announcement of this document. This will normally correspond to the Document Availability (11). However, where further distribution (beyond the audience specified in (11) is possible, a wider announcement audience may be selected.))

13. ABSTRACT (A brief and factual summary of the document. It may also appear elsewhere in the body of the document itself. It is highly desirable that the abstract of classified documents be unclassified. Each paragraph of the abstract shall begin with an indication of the security classification of the information in the paragraph (unless the document itself is unclassified) represented as (S), (C), (R), or (U). It is not necessary to include here abstracts in both official languages unless the text is bilingual.)

The Chip-based Adaptive synthetic aperture radar (SAR) Processor (CHASP) was developed to facilitate the precision processing of airborne SAR data of moving ship targets. CHASP has been extended to support the processing of RADARSAT-1 (R-1) Range Compressed (RC) data and applied to a set of 121 known ships in R-1 Fine mode data.

It is shown that, for R-1 Fine mode data, CHASP-like algorithms can provide more ship information than can be deduced from image analysis alone. Based upon comparison of the ship residual frequency with the Doppler centroid of the background clutter, the ship radial speed can be estimated to within ±2 m/s. Azimuth travelling ships are the most difficult cases for length and speed estimation, but azimuth travelling ships can be readily recognised through a high modulation index of the power envelope in azimuth. The ship radar cross section (RCS) is well estimated for both range and azimuth travelling ships. Unfortunately, processing experiments could neither prove nor refute the expected SAR resolution dependence of the measured ship RCS.

Single look complex (SLC) data could also be used as a starting point for CHASP-like analysis. However, this would introduce additional complexity since the internal details of the SAR processor must be completely known. In general, it is recommend that adaptive ship data analysis start from RC data.

The most important outcome of this work is that, for R-1 Fine mode data, frequency tracking of the ship signature can provide an accurate estimate of the ship radial speed under generalized conditions. Normally, ship radial speed estimation relies upon the azimuth shift of the ship target relative to the ship wake location. Unfortunately, ship wakes are rather rarely visible in R-1 data.

14. KEYWORDS, DESCRIPTORS or IDENTIFIERS (Technically meaningful terms or short phrases that characterize a document and could be helpful in cataloguing the document. They should be selected so that no security classification is required. Identifiers, such as equipment model designation, trade name, military project code name, geographic location may also be included. If possible keywords should be selected from a published thesaurus, e.g. Thesaurus of Engineering and Scientific Terms (TEST) and that thesaurus identified. If it is not possible to select indexing terms which are Unclassified, the classification of each should be indicated as with the title.)

RADARSAT-1, synthetic aperture radar, SAR, fine mode, ship velocity estimation, Automatic Identification System, AIS

Defence R&D Canada

Canada's leader in Defence
and National Security
Science and Technology

R & D pour la défense Canada

Chef de file au Canada en matière
de science et de technologie pour
la défense et la sécurité nationale

www.drdc-rddc.gc.ca